Journal Name

ARTICLE

The crystal structures and mechanical properties of the uranyl carbonate minerals roubaultite, fontanite, sharpite, widenmannite, grimselite and čejkaite†

Received 00th January 20xx,
Accepted 00th January 20xx

DOI: 10.1039/000000x

www.rsc.org/

Francisco Colmenero,[a*] Jakub Plášil,[b] Jiří Sejkora[c]

The research involving the crystal structures and properties of uranyl carbonate minerals is essential in actinide environmental chemistry due to the fundamental role played by these minerals in the migration of actinides from uranium deposits and nuclear waste repositories and in the investigation of accidental site contaminations. In this work, the crystal structure, hydrogen bonding network, X-ray diffraction pattern and mechanical properties of six important uranyl carbonate minerals, roubaultite ($Cu_2[(UO_2)_3(CO_3)_2O_2(OH)_2]\cdot 4\,H_2O$), fontanite ($Ca[(UO_2)_3(CO_3)_2O_2]\cdot 6\,H_2O$), sharpite ($Ca[(UO_2)_3(CO_3)_4]\cdot 3\,H_2O$), widenmannite ($Pb_2[(UO_2)(CO_3)_2(OH)_2]$), grimselite ($K_3Na[(UO_2)(CO_3)_3]\cdot H_2O$) and čejkaite ($Na_4[(UO_2)(CO_3)_3]$), are investigated using first principles solid-state methods based in Density Functional Theory. The determination of the positions of the hydrogen atoms in the unit cells of fontanite, sharpite and grimselite minerals, defining the hydrogen bonding network in their crystal structures, has not been feasible so far due to the low quality of their experimental X-ray diffraction patterns. The full crystal structures of these minerals are obtained here and their hydrogen bonding networks are studied in detail. Furthermore, the experimental structures of roubaultite, widenmannite and čejkaite, obtained by refinement from X-ray diffraction data, are confirmed. In the six cases, the computed unit-cell parameters and the associated geometrical variables are in excellent agreement with the available experimental information. Furthermore, the X-ray diffraction patterns computed from the optimized structures are in satisfactory agreement with their experimental counterparts. The knowledge of the full crystal structures, being extraordinarily relevant for many scientific fields, is also extremely interesting because it opens the possibility of determining their physico-chemical properties using the first principles methodology. The measurement of these properties under safe conditions is very expensive and complicated due to the radiotoxicity of these minerals. In this paper, a large set of relevant mechanical properties of these minerals are determined including their bulk, shear and Young moduli, the Poisson's ratio, ductility, hardness and anisotropy indices and bulk modulus pressure derivatives. These properties have not been measured so far and, therefore, are predicted here. Four of these minerals, roubaultite, fontanite, sharpite and widemmannite, are highly anisotropic and exhibit negative mechanical phenomena under the effect of small external pressures.

1 Introduction

The study of the crystal structures and physico-chemical properties of uranyl carbonate minerals[1-19] is extremely important in actinide environmental chemistry.[1-2,12-14,20-29] The knowledge of their precipitation/dissolution processes is fundamental to describe the mobility of actinides in the environment.[1-7,12-16,18.22-29] Carbonate and bicarbonate ions, present in significant concentrations in many natural groundwaters, are extraordinarily strong complexing agents for actinides and, therefore, the carbonate complexes of uranium[1-2,4,7,12-14,30-46] play an important role in the migration from nuclear waste repositories[1,5,8,12-16,19,47-52] or in the accidental site contaminations.[53-61] Aqueous uranyl carbonate complexes are the most prominent uranium species in circumneutral to alkaline natural waters in which carbonate or bicarbonate ions are present or contain significant amounts of dissolved carbon dioxide.[2,5,7] Uranyl carbonate minerals precipitate from these solutions where evaporation is significant or the partial pressure of carbon dioxide is substantial.[5,14,62] The finding of natural uranyl carbonate minerals advise of the possible existence of large concentrations of uranium in surface or underground waters and, therefore, their study and precise characterization by X-ray diffraction methods or spectroscopic

[a] *Instituto de Estructura de la Materia (IEM-CSIC). C/ Serrano, 113 – 28006 Madrid – Spain. Orcid number: F. Colmenero: https://orcid.org/0000-0003-3418-0735.*
[b] *Institute of Physics ASCR, v.v.i., Na Slovance 2, 182 21, Praha 8, Czech Republic. Orcid number: J. Plášil: https://orcid.org/0000-0001-6627-5742.*
[c] *Mineralogicko-petrologické oddělení, Národní muzeum, Cirkusová 1740, 193 00 Praha 9, Czech Republic. Orcid number; J. Sejkora: https://orcid.org/0000-0003-2763-2043.*

† Electronic Supplementary Information (ESI) available: (a) Material data and calculation parameters; (b) Interatomic distances and angles; (c) Positions of the main reflections in the X-ray diffraction patterns; (d) Unit-cell volumes and lattice parameters under isotropic and anisotropic pressures; (e) Computed positions of the atoms in the unit cell of roubaultite (CIF file): CCDC 1998009; (f) Computed positions of the atoms in the unit cell of fontanite (CIF file): CCDC 1998010; (g) Computed positions of the atoms in the unit cell of sharpite (CIF file): CCDC 1998013; (h) Computed positions of the atoms in the unit cell of widenmannite (CIF file): CCDC 1998014; (i) Computed positions of the atoms in the unit cell of grimselite (CIF file): CCDC 1998015; (j) Computed positions of the atoms in the unit cell of čejkaite (CIF file): CCDC 1998011; CCDC deposition numbers: 1998009-1998011 and 1998013-1998015. For ESI and crystallographic data in CIF format, see DOI:10.1039/000000x.

techniques is very important. However, the current state of the knowledge about the crystal structures, vibrational spectra, physico-chemical properties and thermodynamic stability of uranyl carbonate minerals is quite limited. Their study is also essential for understanding the paragenetic sequence of minerals arising from the oxidative dissolution processes occurring in uranium deposits[5,14,18,62-64] and from corrosion of spent nuclear fuel in deep geological disposal repositories for nuclear waste. [1,5,8,12-16,19,47-52] Furthermore, the knowledge of the crystal structures of uranyl-containing minerals is crucial to evaluate the possible incorporation of fission products and transuranic elements into their structures.[65-71]

Twenty-nine natural uranyl carbonate minerals[7,10,17-18] have been described so far. However, due to the lack of material suitable for crystallographic study and the difficulties encountered in the corresponding X-ray diffraction studies, the full crystal structures of these minerals have been published only for a relatively small subset of them. Difficulties result in many cases from the relatively poor quality of the crystal samples, the presence of twinning, the severe overlap of some reflections and other X-ray diffraction artifacts. Due to these difficulties, the structures which have been published so far have frequently a quality lower than usual for uranyl minerals, which is manifested by the large bond-length errors encountered. Despite the difficulties, a large amount of effort[72-93] has been devoted by several reputed French and German mineralogists[72-77] and the research groups from Notre Dame, USA,[9-11,78-80] and Prague, Czech Republic,[17-18,81-91] to the determination of the crystal structures of these minerals. In most cases, only the crystal structures excluding the positions of the hydrogen atoms present in their unit cells have been reported. A simple illustration is provided in this work. For the six mineral species considered in this paper, the full crystal structures of only three of them are known, roubaultite,[73] widenmannite[85] and čejkaite,[90] and the later one does not contain hydrogen in its crystal structure. For fontanite,[78] sharpite[83] and grimselite,[86] the positions of the hydrogen atoms are unknown. The problem may be lifted using first principles solid-state methods which have been successfully applied for the determination of the full crystal structures of many important uranyl-containing minerals, such as schoepite,[94] metaschoepite,[95] becquerelite,[96] kasolite,[97] uranophane-β,[98] vandenbrandeite,[99] uranosphaerite,[100] bayleyite[101] and uranopilite.[102] The first principles determination of the crystal structures of materials is being increasingly important in an enormous range of physical problems such as the development of photovoltaic, thermoelectric and magnetic devices.[103-105]

The partial knowledge of the crystal structures of many important uranyl minerals, or even its complete ignorance, is a significant drawback because the positions of the hydrogen atoms specify the hydrogen bonding network in these structures. Hydrogen bonding is, for the majority of these minerals, one of the most important bonding type maintaining linked the structures and is an essential factor determining their relative stabilities. A further important consequence is the impossibility of using these partial structures as a starting point for accurate first principles solid-state computations.[94-102,106-126] Information provided by these computational treatments has been shown to be extremely rich in recent years, providing fresh new methods for spectroscopic assignment and interpretation of the results of experimental studies.[94,97-102,113-117,121-122,126] The achievement of this information is impossible from the use of experimental techniques and the theoretical methodology has allowed the safe and accurate prediction of highly relevant material properties of these minerals, such as their mechanical properties and thermodynamic functions,[94-102,107-108,110,113,116-125] from first principles, that is, in the complete absence of experimental information. The experimental determination of these properties could be exceedingly tricky, due to the radiotoxicity of these minerals, and extremely expensive. Two of the most important features allowing the use of the first principles methodology are the increased availability of highly efficient supercomputer installations and the implementation of new, improved theoretical techniques in sophisticated solid-state codes.[127-132] Furthermore, the seminal generation of an accurate scalar-relativistic norm-conserving pseudopotential for uranium atom[113-114] reduced the computational expense of the calculations enormously, increased the range of compounds amenable to theoretical study and increased the precision of the results obtained from the first principles calculations.

The most technically challenging computational study performed up to date has been the recent theoretical study of the uranyl carbonate mineral bayleyite, containing eighteen water molecules per formula unit.[101] Despite the extreme complexity of the unit cell of this mineral, the results obtained for its crystal structure, hydrogen bonding network geometry and infrared spectra were extraordinarily satisfactory. The good quality of the results and those obtained previously for the rutherfordine mineral,[114,118,124] strongly stimulated the present study involving the determination of the crystal structures and properties of an extended set of uranyl carbonate minerals. In this work, the crystal structures and mechanical properties of six important uranyl carbonate minerals are investigated using first principles methods. A highly visual approach is used in order to make comprehensive the intricate crystal structures and mechanical properties of these minerals, which otherwise can only be understood by experts. Furthermore, the structure-function relationships between the computed crystal structures and mechanical properties are studied. It will be shown that four of these minerals, roubaultite, fontanite, sharpite and widenmannite, have very high mechanical anisotropies and display negative mechanical phenomena under the effect of small external pressures. The materials exhibiting these phenomena have an immense range of interesting potential applications resulting specifically from their mechanical behavior.[133-141]

This paper is organized as follows. In Section 2, the first principles solid-state methodology employed in this work is described. The computed crystal structures and mechanical properties are reported in Section 3. For the six uranyl carbonate minerals studied, the calculated structures are carefully compared with the experimental structures and the hydrogen bonding network derived from the computed positions of the atoms in the corresponding unit cells is

described. The X-ray diffraction patterns derived from the computed and experimental crystal structures are also contrasted. Finally, the computed stiffness tensors and mechanical properties are reported. The conclusions of this work are presented in the last Section 4.

2 Theoretical solid-state methods

The crystal structures and mechanical properties of the six uranyl carbonate minerals considered, roubaultite, fontanite, sharpite, widenmannite, grimselite and čejkaite, were determined by using the CASTEP (Cambridge Serial Total Energy Program) code ,[127] interfaced with the Materials Studio program suite.[142] Periodic Density Functional Theory based on plane wave basis sets and pseudopotentials to describe the internal atomic electrons[143] was utilized. The specific pseudopotentials employed in the calculations were norm-conserving pseudopotentials[144] from CASTEP package for all the atoms involved in the unit cells of the minerals studied except for uranium, for which a scalar-relativistic norm-conserving pseudopotential constructed from first principles[113-114] was utilized. The overall quality of this pseudopotential has been verified extensively for the computation of the crystal structures, vibrational spectra and properties of uranium-containing materials.[94-102,113-126] The material data and calculation parameters employed in the calculations are provided in Table S.1 of the ESI.† The computed full crystal structures are also given in the ESI† as files with CIF (Crystallographic Information File) format. The computations were performed using the Perdew-Burke-Ernzerhof (PBE) energy-density functional[145] complemented with Grimme's empirical dispersion correction[146] for all the hydrogen-containing minerals and the PBEsol functional[147] for čejkaite. The superiority of PBEsol functional[147] with respect to the PBE[145] one for materials in which hydrogen bonding is not present has been documented in several previous works,[114,117-118,124,148-149] the study of the uranyl carbonate mineral rutherfordine[114,118,124] and uranium trioxide[117] being particularly relevant for the present study. The Hubbard correction,[150] improving the description of the strong Coulomb repulsion between electrons occupying f orbitals in materials containing uranium with IV oxidation state,[151-153] was not used because its impact in the computed crystal structures was exceedingly small. Trial calculations of the vibrational spectra of these minerals with this correction also led to results which were almost identical to those obtained without Hubbard correction, in line with many previous studies in materials in which uranium exists with VI oxidation state.[94-102,106-126]

The unit-cell parameters and the positions of the atoms in the unit cell of the uranyl carbonate minerals under consideration were fully optimized using the Broyden–Fletcher–Goldfarb–Shanno (BFGS) technique.[154] All the crystal structure optimizations were carried out with stringent convergence thresholds in the variation of the total energy, maximum atomic force, maximum atomic displacement and maximum stress of 0.5×10^{-5} eV/atom, 0.01 eV/Å, 0.5×10^{-3} Å and 0.02 GPa, respectively. The experimental crystal structures of roubaultite,[73] widenmannite[85] and čejkaite[90] were directly employed as the initial input for the geometrical optimization. Since for fontanite,[78] sharpite[83] and grimselite[86] the structures were only partially known, several different trial sets of hydrogen atoms at approximate positions in the corresponding unit cells were introduced before optimization. All the structures resulting from the different sets of initial positions of the hydrogen atoms were then fully optimized using the BFGS method. Several possible structures were obtained in some cases, but all of them except one were rejected using energy criteria. The positiveness of the energy second-derivative matrix (Hessian) matrix was verified for all the final structures. The X-ray diffraction patterns of the minerals studied were obtained[155] from the experimental (in some cases incomplete[78,83,86]) and computed crystal structures using the software REFLEX included in Materials Studio program suite.[142]

The matrix elements of the stiffness or elasticity tensor[156] were determined using the technique of finite deformations[157]. This technique appears to be more effective for this purpose than density functional perturbation theory and the energy-based methods.[157] It has been extensively utilized for the computation of the elastic response of many solid materials.[93,96-102,116,118,121-122,124-125,158-162] The tridimensional representations of the mechanical properties as a function of the direction of the applied strain for the six uranyl carbonate minerals studied in this work were obtained using the ElAM code.[163]

The crystal structures of the minerals studied were fully optimized under the effect of seventeen different external isotropic pressures with values in the range −1.0 to 9.0 GPa. The pressure-volume data was fitted to a 4th order Birch-Murnaghan equation of state (4-BM-EOS).[164] From the values of the fit parameters, the derivatives of the bulk modulus with respect to pressure were determined. The fits of the pressure-volume data to the selected equation of state were carried out employing Angel's EOSFIT 5.2 software.[165-166] The structure optimizations under pressure were also performed using the BFGS method.[154]

3. Results and discussion

3.1 Unit-cell parameters

The computed unit-cell parameters associated with the crystal structures of the uranyl carbonate minerals investigated in this paper are given in Table 1. The results are in excellent agreement with the unit-cell parameters obtained from experimental measurements for all the materials considered. As can be seen in Table 1, the experimental unit-cell volumes for roubaultite,[73] fontanite,[78] sharpite,[83] widenmannite,[85] grimselite[86] and čejkaite[90] are only 2.0, 0.2, 2.6, 2.6, 1.6 and 1.3%, respectively. The computed unit cell volumes obtained using the uncorrected PBE functional for the first five minerals are 4.4, 1.9, 5.4, 4.6 and 5.5%, respectively. Therefore, the results are improved significantly when dispersion corrections are included as a result of the better description of the hydrogen bonding network present in the crystal structures of these minerals. For čejkaite, the results obtained with the PBEsol functional are excellent, in line with results obtained for other anhydrous uranyl-containing materials as rutherfordine[114,118,124] and γ-uranium trioxide.[117]

Journal Name

ARTICLE

Table 1. Unit-cell parameters of the selected uranyl carbonates. The theoretical and experimental results correspond to the zero and room temperatures, respectively.

Parameter	α (Å)	b (Å)	c (Å)	α (deg)	β (deg)	γ(deg)	Vol. (Å^3)	Dens. (gr/cm^3)
Roubaultite								
PBE	6.9914	7.9146	7.9801	91.22	91.83	95.04	439.505	4.516
PBE+disp	6.9481	7.8252	7.9303	90.93	91.73	94.46	429.595	4.620
Exp.[73]	6.924(3)	7.767(3)	7.850(3)	90.89(4)	92.16(4)	93.48(4)	421.018	4.714
Exp.[72]	6.87	7.73	10.87	134.12	86.29	93.10	-	-
Fontanite								
PBE	6.9959	17.5655	15.3469	90.0	89.25	90.0	1885.743	3.911
PBE+disp	6.9675	17.3943	15.2523	90.0	89.36	90.0	1848.382	3.990
Exp.[78]	6.968(3)	17.276(7)	15.377(6)	90.0	90.064(6)	90.0	1851.069	3.984
Sharpite								
PBE	5.0020	15.9008	22.4137	90.0	90.0	90.0	1782.692	4.204
PBE+disp	4.9836	15.7296	22.1367	90.0	90.0	90.0	1735.300	4.319
Exp.[83]	4.9032(4)	15.6489(11)	22.0414(11)	90.0	90.0	90.0	1691.230	4.407
Widenmannite								
PBE	4.9687	9.6332	9.1466	90.0	90.0	90.0	437.794	6.361
PBE+disp	4.9598	9.5494	9.0651	90.0	90.0	90.0	429.351	6.486
Exp.[85]	4.9770(7)	9.3869(13)	8.9597(12)	90.0	90.0	90.0	418.585	6.653
Exp.[76]	4.95	9.36	8.99	90.0	90.0	90.0	416.52	6.69
Exp.[93]	5.002(2)	9.381(2)	8.971(3)	90.0	90.0	90.0	420.953	6.615
Exp.[84]	5.007(4)	9.378(6)	8.964(4)	90.0	90.0	90.0	420.910	6.616
Exp.[84]	5.001(3)	9.381(2)	8.960(2)	90.0	90.0	90.0	420.353	6.625
Grimselite								
PBE	9.5700	9.5700	8.3822	90.06	90.07	121.73	652.985	3.094
PBE+disp	9.3839	9.3839	8.4130	90.07	90.07	121.93	628.738	3.213
Exp.[86]	9.2507(1)	9.2507(1)	8.1788(1)	90.0	90.0	120.0	606.135	3.333
Exp.[79]	9.302(2)	9.302(2)	8.260(3)	90.0	90.0	120.0	618.961	3.264
Exp.[77,92]	9.29	9.29	8.26	90.0	90.0	120.0	617.36	3.27
Čejkaite								
PBEsol	9.3203	16.1291	6.4978	90.0	91.25	90.0	976.588	3.686
Exp.[90]	9.2919(8)	16.0991(11)	6.4436(3)	90.0	91.404(5)	90.0	963.627	3.736

3.2 Structure and hydrogen bonding

3.2.1 Roubaultite, $Cu_2[(UO_2)_3(CO_3)_2O_2(OH)_2]\cdot 4\,H_2O$

3.2.1.1 Crystal Structure

Roubaultite was described for the first time in 1970 by Cesbron *et al*.[72] from a natural sample collected from Shinkolobwe mine (Shaba province, Democratic Republic of the Congo, DRC). It was named in honor of Marcel Roubault, a French geologist and professor of the National School of Geology in Nancy, France, and a pioneer in uranium research in France. It has been also encountered in the Mussonoi and Kamoto mines, from Shaba province, DRC, and in the Komsomol ore field, eastern Siberia, Russia. It is frequently found in the oxidation zone of copper-bearing uranium deposits, formed by alteration of uraninite. This mineral was initially described[72] as a copper uranate with formula unit $Cu_2(UO_2)_3(OH)_{10}\bullet 5\,H_2O$. Its true composition, $Cu_2[(UO_2)_3(CO_3)_2O_2(OH)_2]\cdot 4\,H_2O$, and its crystal structure were reported in 1985 by Ginderow and Cesbron[73] from a natural sample from Shinkolobwe mine.

The computed crystal structure of roubaultite is shown in Fig. 1. The structure of roubaultite is extraordinarily interesting because, as in the case of fontanite mineral (see below), the uranium atoms display the hexagonal and pentagonal bipyramidal coordination types within the same structure.[73] The coordination environment of uranium in the pentagonal bipyramids is formed by the two uranyl (apical) oxygen ions and four oxygen and one hydroxyl ions in the equatorial plane ($UO_2[O_4(OH)]$). For the hexagonal bipyramids, all the ligands are oxygen ions ($UO_2[O_6]$). The copper and carbon atoms show octahedral and planar triangular coordination, respectively. In the copper octahedra, the two apical oxygen atoms belong to water molecules and two of the equatorial oxygens copper atom are from hydroxyl ions. Thus, the coordination polyhedra of copper in roubaultite may be expressed as $CuO_2(OH)_2(H_2O)_2$. The copper octahedra are very distorted, the apical distances (about 2.5 Å) being much larger than the equatorial distances (about 2.0 Å). A similar coordination polyhedron is present in the copper atoms of vandenbrandeite mineral.[99] The basic building units in the structure of roubaultite are shown in Fig. 1.C.

The crystal structure or roubaultite is formed of two types of parallel chains expanding along [100] crystallographic direction. The first type of chain contains alternating hexagonal bipyramids and dimers formed from two pentagonal

bipyramids, as shown in Fig. 1.B. The second type of chain is composed of edge-sharing copper octahedra. The chains are linked laterally by sharing an equatorial vertex (hydroxyl ion) of the uranium pentagonal bipyramid dimers with an equatorial vertex of the copper octahedra and by means of carbonate triangles, which share an edge with a uranium hexagonal bipyramid and an equatorial vertex of a copper octahedra. The chains form copper uranyl carbonate layers stacked perpendicularly to (011) plane. The structure of the layers in roubaultite has not been found in any other uranyl mineral, and form the basis for the roubaultite anion-sheet topology.[11] The hydrogen bonding connecting the hydroxyl ions and water molecules coordinating the copper atom in a given layer and the uranyl apical oxygen atoms of an adjacent layer is the unique bonding mechanism keeping together the layers in roubaultite.

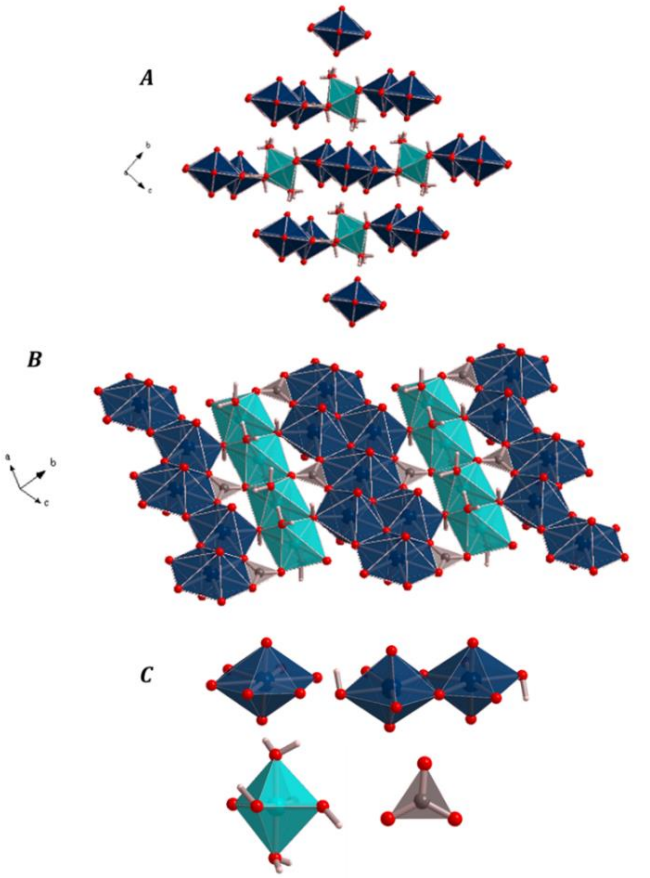

Fig. 1. The computed crystal structure of roubaultite: (A) View of a 2 × 2 × 1 supercell from [100]. The *b* and *c* axes are rotated 90° to show the copper uranyl carbonate layers horizontally; (B) View of an isolated copper uranyl carbonate layer; (C) The basic building units in the structure of roubaultite: the uranyl hexagonal bipyramid, the uranyl pentagonal bipyramid dimer, the copper distorted octahedron and the carbonate triangle. Color code: U - Dark blue; Cu - Clear blue; C - Gray; O - Red; H - White.

There are two symmetry non-equivalent uranium atoms in roubaultite (referred to as U1 and U2). The U1 atoms display hexagonal bipyramidal coordination and the U2 atoms show pentagonal bipyramidal coordination.[73] All the copper and carbon atoms are symmetry equivalent (simply referred to as Cu and C in this paper, respectively). The calculated crystal structure of roubaultite was carefully benchmarked against the experimental structure.[73] The interatomic distances and angles derived from the computed atomic positions are given in Tables S.2 and S.3 of the ESI.† The computed average apical and equatorial U-O distances are 1.84 and 2.45 Å for the U1 atoms and 1.81 and 2.35 Å for U2. These values are in excellent agreement with the experimental values of 1.82(1) and 2.44(1) Å for U1 and 1.80(1) and 2.35(1) Å for U2. These values may also be compared with the average values obtained by Burns *et al.*[9] from an extensive series of well-refined crystal structures in which uranium display hexagonal bipyramidal (1.78(3) and 2.37(9) Å) and pentagonal bipyramidal (1.79(4) and 2.37(4) Å) coordination. The calculated average C-O and Cu-O distances are 1.29 and 2.23 Å, which can be compared to their experimental counterparts[73] of 1.29(2) and 2.15(2) Å, respectively.

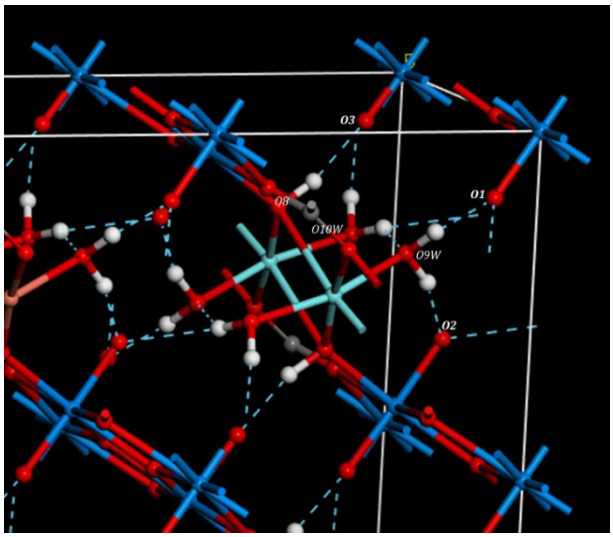

Fig. 2. Hydrogen bond structure in the computed crystal structure of roubaultite. Color code: U - Dark blue; Cu - Clear blue; C - Gray; O - Red; H - White.

3.2.1.2 Hydrogen bonding

There are two non-equivalent water molecules in the unit-cell of roubaultite, denoted as W9 and W10. They form part of the coordination structure of the copper atom and are located at the apical positions of the copper octahedra. The computed hydrogen bond structure is shown in Fig. 2. As can be seen in Tables S.2 and S.3 (and Fig.2), there are six non-equivalent hydrogen bonds. In the first hydrogen bond, O8-H1···O3, the donor oxygen atom, O8, is from a hydroxyl ion and the acceptor oxygen atom, O3, is an apical oxygen atom from a uranyl pentagonal bipyramid of an adjacent layer. The second and third ones, O9W-H3···O2' and O9W-H2···O1, link the oxygen atom of the W9 water molecule with an apical oxygen atom from a pentagonal bipyramid of the same layer (O2') and an apical oxygen atom of a pentagonal bipyramid of and adjacent layer (O1), respectively. In the rest of hydrogen bonds, O10W-H4···O9W, O10W-H4···O2 and O10W-H5···O1, the donor oxygen atoms belong to the water molecule W10 and the acceptor ones

are from the other water molecule, W9, and from the uranyl hexagonal (O1) and pentagonal (O2) bipyramids of an adjacent layer. Thus, four of the hydrogen bonds act as the glue linking two adjacent copper uranyl carbonate layers, one reinforces the link between the copper octahedra and uranyl bipyramids of the same layer, and one strengthens the hydrogen bond structure itself.

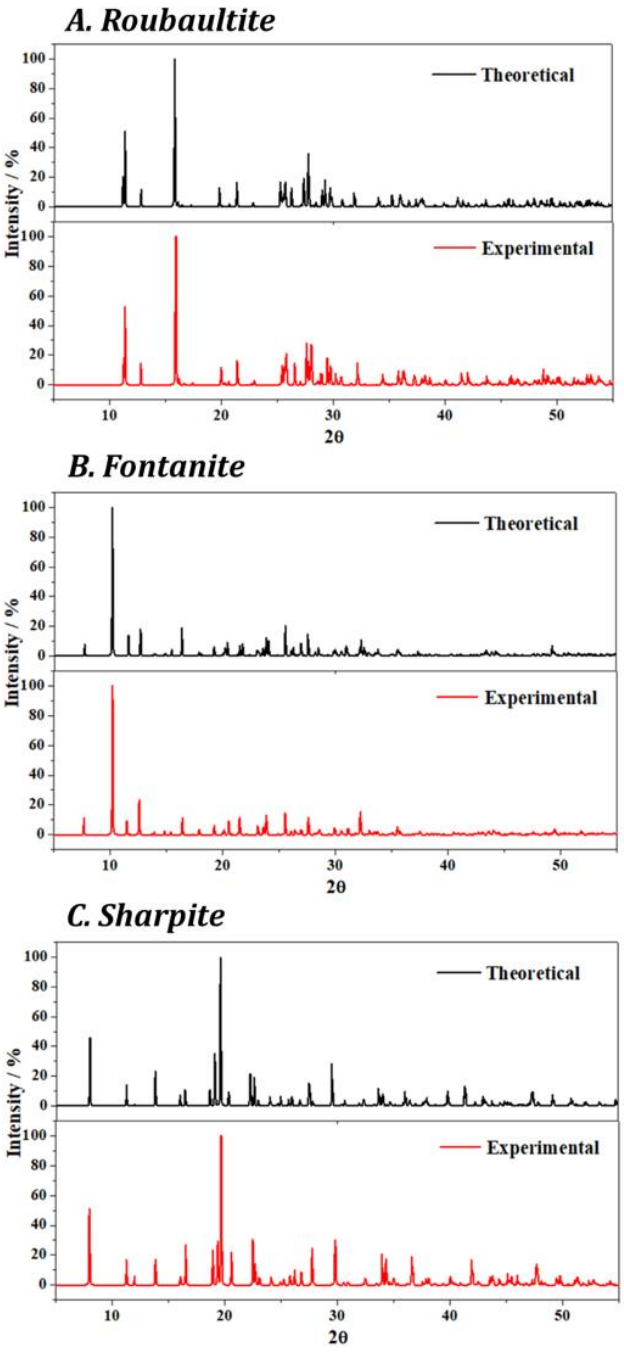

Fig. 3. X-ray diffraction patterns of the uranyl carbonate minerals roubaultite, fontanite and sharpite using $\mathbf{CuK_\alpha}$ radiation (λ = 1.540598 Å). For each mineral, the upper pattern is derived from the computed crystal structure and the lower one is generated from the experimental crystal structures.[73,78,83]

3.2.1.3 X-ray diffraction pattern

From the energy-optimized and experimental[73] crystal structures, the X-ray diffraction patterns of roubaultite were calculated using $\mathrm{CuK_\alpha}$ radiation (λ = 1.540598 Å) utilizing the program REFLEX belonging to the Materials Studio program suite.[142] The resulting patterns are compared in Fig. 3.A. The computed and experimental patterns are highly consistent. The consistency of the theoretical and experimental patterns can be evaluated in a more detailed form from Table S.4 of the ESI,† giving the precise values of the positions of the main reflections in both patterns. As can be seen, the differences are very small, the largest deviation being $\Delta(2\theta) \sim 0.5°$ for the [2 -2 1] reflection.

3.2.2 Fontanite, $\mathbf{Ca[(UO_2)_3(CO_3)_2O_2] \cdot 6\,H_2O}$

3.2.2.1 Crystal Structure

Fontanite is a hydrated calcium uranyl carbonate mineral, which was first described in 1992 by Deliens and Piret[74] from a natural mineral found in Rabejac, Hèrault, France. They provided a formula unit for fontanite of $\mathrm{Ca(UO_2)_3(CO_3)_4 \cdot 3\,H_2O}$. The composition and definitive crystal structure were later reported by Hughes and Burns[78] in 2003, who analyzed the holotype for fontanite from Rabejac, France, and gave the true composition $\mathrm{Ca(UO_2)_3(CO_3)_2O_2 \cdot 6\,H_2O}$. The name of the mineral was coined after Francois Fontan, a mineralogist from the University of Paul-Sabatier, Toulouse, France. However, these authors were not able to determine the complete crystal structure of this mineral, including the positions of the hydrogen atoms.[77] The full crystal structure is reported in this work.

The computed crystal structure of fontanite is shown in Fig. 4. As for roubaultite, the hexagonal and pentagonal bipyramidal coordination types around the uranium atoms are simultaneously displayed in the same structure.[74,78] In fontanite, the coordination environment of uranium in the pentagonal/hexagonal bipyramids is formed by the two uranyl (apical) oxygen atoms and five/six oxygen atoms in the equatorial plane. The calcium atom is coordinated with six oxygen atoms from six different water molecules and two uranyl (apical) oxygens, one belonging to a uranyl pentagonal bipyramid and the other to a uranyl hexagonal bipyramid. Thus, the coordination number of calcium in fontanite is eight and its coordination environment can be described as $\mathrm{CaO_2(H_2O)_6}$. The carbon atom and three oxygen atoms form carbonate groups which, as usual, are arranged in a planar triangular structure.

In the structure of fontanite, the uranyl bipyramids are arranged in chains expanding along [100]. These chains are formed by alternate hexagonal bipyramids and dimers formed with two pentagonal bipyramids as shown in Fig. 4.D. The chains are relatively similar to those found for roubaultite in Section 3.2.2.1, but the linkage of the chains in the structure is different. The chains are linked laterally by sharing carbonate triangles; two opposite equatorial edges of each hexagonal bipyramid are shared with carbonate groups, one on either side of the chain. The remaining oxygen atom at the other vertex of the carbonate triangles is shared with a uranyl pentagonal bipyramid of an

adjacent chain. The uranyl chains linked with the carbonate triangles form uranyl carbonate sheets or layers, as shown in Figs. 4.C and 4.D. The adjacent uranyl chains are not linked in a planar way. The view of the uranyl chains seen from [100] (Fig. 4.C) shows that the chains are tilted one respect to the other and arranged in a zig-zag form. The uranyl carbonate layers in fontanite have a structure that belongs to the phosphuranylite anion topology.[78,11] Fontanite mineral is the only uranyl carbonate mineral whose structure is based on this anion topology.[78] The calcium atoms, located in the interlayer space between two adjacent uranyl carbonate sheets, are bonded to one uranyl ion from each of the two adjacent sheets and provide the main bonding mechanism between them. The calcium atom is coordinated with six additional water molecules, which are linked through hydrogen bonds to the upper and lower uranyl carbonate layers giving an additional bonding mechanism between the layers. The hydrogen bond network structure in fontanite is described in this paper for the first time because it has not been revealed by X-ray or neutron diffraction data up to date.

There are three symmetry non-equivalent uranium atoms in fontanite, referred to as U1, U2 and U3. The uranium atoms denoted as U1 display hexagonal bipyramidal coordination and the atoms U2 and U3 show pentagonal bipyramidal coordination. The calcium atoms in fontanite belong to a single symmetry equivalence class. Finally, there are two symmetry non-equivalent carbon atoms (C1 and C2). The interatomic distances and angles derived from the calculated positions of the atoms in the unit cell of fontanite are given in Tables S.5 and S.6 of the ESI,† together with the corresponding experimental values for the non-hydrogen atoms. The experimental average apical U-O distances for the U1, U2 and U3 atoms are 1.80(3), 1.73(3) and 1.75(3) Å and the calculated ones are 1.817, 1.826 and 1.826 Å, respectively. The experimental and calculated average Ca-O distances are in good agreement (2.51(4) and 2.498 Å). Finally, the experimental average C1-O and C2-O distances, 1.29(4) and 1.29(4) Å, are extremely close to the computed values which are equal and have a value of 1.289 Å.

3.2.2.2 Hydrogen bonding

There are six non-equivalent water molecules in fontanite. These water molecules are denoted as W4, W15, W16, W17, W18 and W19. All these water molecules participate directly in the coordination environment of the calcium atom and are placed in the interlayer space between the uranyl carbonate layers. The computed hydrogen bond structure is shown in Fig. 5. As can be observed in Table S.7 of the ESI,† there are eleven non-equivalent hydrogen bonds in fontanite. Table S.7 contains the calculated hydrogen bond parameters. The two hydrogen bonds O4W-H2···O4W and O16W-H6···O19W link two different interlayer molecules, and, therefore, serve as support for the hydrogen bond network. The remaining nine hydrogen bonds link the apical uranyl oxygen atoms with the interlayer water molecules, which, in turn, are linked to the interstitial calcium atoms. Thus, while the direct bonds of the calcium atoms with the uranyl oxygens have the primary function of keeping together the layers of fontanite, the hydrogen bonding network act as a reinforcement of the layered structure.

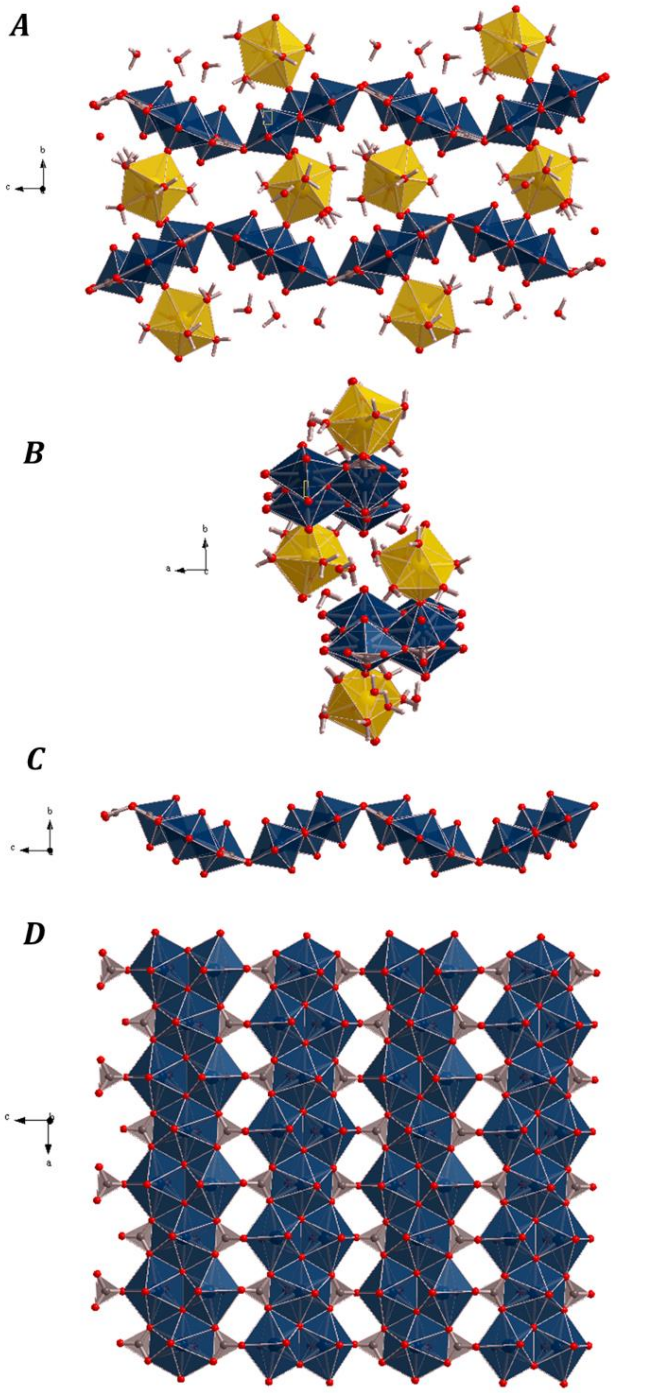

Fig. 4. The computed crystal structure of fontanite. The views provided in the figure are from a 4 × 1 × 2 supercell: (A) View from [100]; (B) View from [001]; (C) View of an isolated uranyl carbonate sheet from [100]; (D) View of an isolated uranyl carbonate sheet from [010]. Color code: U - Blue; Ca - Yellow; C- Gray; O - Red; H - White.

3.2.2.3 X-ray diffraction pattern

The X-ray diffraction patterns of fontanite derived from the energy-optimized and experimental[78] structures (CuK_α radiation) are compared in Fig. 3.B. A high degree of consistency

is observed. The positions of the most intense reflections in the theoretical and experimental patterns are given in Table S.8 of the ESI.† The differences are satisfactorily small, the largest deviation being $\Delta(2\theta) \sim 0.4°$ for the [-1 1 5] reflection.

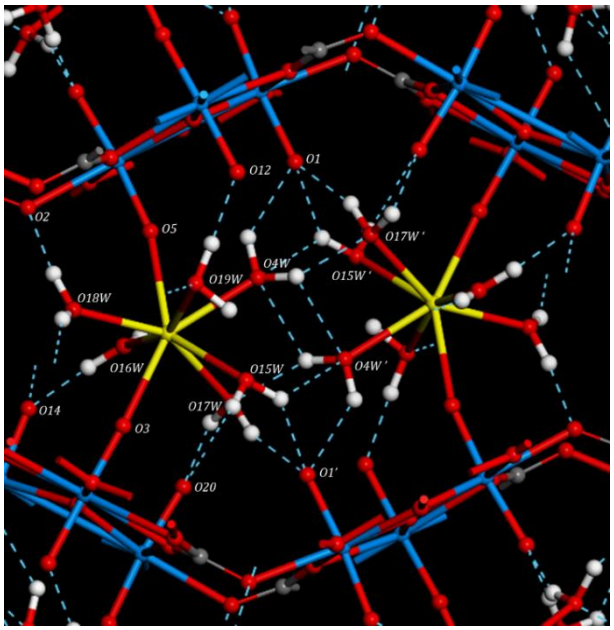

Fig. 5. Hydrogen bond structure in the computed crystal structure of fontanite. Color code: U - Blue; Ca - Yellow; C- Gray; O - Red; H - White.

3.2.3 Sharpite, $Ca[(UO_2)_3(CO_3)_4] \cdot 3\,H_2O$

3.2.3.1 Crystal Structure

Sharpite, $Ca[(UO_2)_3(CO_3)_4] \cdot 3\,H_2O$, is, as fontanite, a hydrated calcium uranyl carbonate mineral. However, its water content is smaller than that of fontanite since it has three water molecules per formula unit only. Sharpite was encountered for the first time 1938 by Mélon[167] in Shinkolobwe mine (Shaba province, DRC) and described it as a hydrated rutherfordine mineral, $UO_2 \cdot CO_3 \cdot 4/3 \cdot H_2O$. This author named the mineral as sharpite after major R. R. Sharp, which discovered the uranium deposit of Shinkolobwe in 1915. Sharpite was then reported from several localities worldwide. The chemical composition of sharpite remained unknown until 1984, when a more complete compositional and spectroscopic study was carried out by Čejka *et al*.[82] The crystal structure of this mineral was recently established by Plášil[83] (2018). However, the determination of the full crystal structure, including the positions of the hydrogen atoms, was not feasible and is reported here.

The computed crystal structure of sharpite is displayed in Fig. 6. There are two uranium (U1 and U2), two carbon (C1 and C2), and one calcium (Ca) symmetrically non-equivalent atoms in its unit cell. Uranium atom (U1 and U2) in sharpite shows uranyl hexagonal bipyramidal coordination and the carbon atoms (C1 and C2) are arranged in planar carbonate triangles. The unit-cell site associated with the C2-type atoms appears to be partially occupied,[83] but the corresponding occupation is high (larger than 75%). The calcium atom is coordinated by eight ligands, four of them being oxygen atoms belonging to water molecules and the remaining ones being uranyl bipyramid equatorial oxygen atoms. The shape of the calcium atom coordination polyhedron in sharpite is quite unusual and is shown in Fig. 6.E.

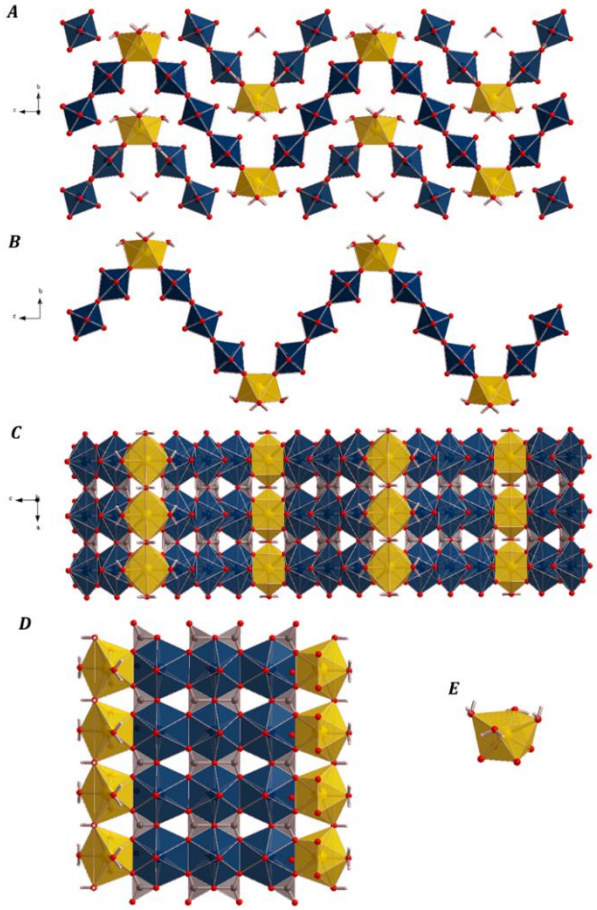

Fig. 6. The computed crystal structure of sharpite. The views provided in the figure are from a 4 × 1 × 2 supercell: (A) View from [100]; (B) View of an isolated zig-zag layer from [100]; (B) View of an isolated zig-zag layer from [010]; (D) View of an edge of the zig-zag layer; (E) Calcium atom coordination polyhedra. Color code: U - Blue; Ca - Yellow; C - Gray; O - Red; H - White.

In sharpite,[83] each U2 uranyl hexagonal bipyramid shares two opposite equatorial edges with two U1 bipyramids forming U1–U2–U1 trimers as shown in Fig. 6.D. The trimers form bands by sharing three equatorial upper vertices with the upper trimer and three equatorial lower vertices with the lower one. The spaces between the trimers are occupied by carbon atoms forming carbonate triangles. These triangles occupy only half of the space and leave triangular empty spaces. The structure of these uranyl carbonate bands is related to the structure of the uranyl carbonate sheets in rutherfordine mineral.[114] However, the triangles of a given sheet of rutherfordine are all oriented in the same way. For sharpite, as can be seen in Fig. 6.D, the two triangles at the left-hand side point to the right, and the two triangles at the right-hand side point to the left. A given band is terminated at both sides by calcium polyhedral, which link the band with other two bands forming a zig-zag layer, as shown in Figs. 6.B and 6.C. The calcium polyhedra, therefore, form part

of the layers within sharpite structure, in contrast to its role in many other uranyl minerals in which calcium participates as a pure interlayer cation.[98] Therefore, while sharpite displays an exciting and unusual crystal structure, also has some common features with the structure of rutherfordine.[83,114]

The computed bond distances and angles between the atoms in the unit cell of sharpite are compared with the experimental values in Tables S.9 and S.10 of the ESI.† The experimental average apical U-O distances for the U1 and U2 atoms are 1.760(17) and 1.769(19) Å and the calculated ones are 1.794 and 1.825 Å, respectively. Similarly, the experimental average distances from uranium to the equatorial oxygen atoms are 2.468(18) and 2.445(11) Å for the U1 and U2 atoms and the corresponding calculated distances are 2.565 and 2.472 Å, respectively. The experimental and calculated average Ca-O distances are 2.489(10) and 2.543 Å, respectively. Finally, the experimental average C1-O and C2-O distances, 1.285(13) and 1.409(16) Å, are satisfactorily reproduced theoretically, the computed values being 1.290 and 1.352 Å, respectively.

3.2.3.2 Hydrogen bonding

The computed hydrogen bonding network in sharpite is shown in Fig. 7. The computed hydrogen bond parameters are given in Tables S.9 and S.10. Two adjacent zig-zag layers in sharpite are held together by means of a network of hydrogen bonds linking the oxygen atoms in the water molecules coordinating the calcium atoms of a given layer (W7 and W8) with the apical oxygen atoms of the uranyl hexagonal bipyramids (O5 and O3) of the other. There are two nonequivalent hydrogen bonds in sharpite, O7W-H7···O5 and O8W-H8···O3. The two hydrogen bonds arising from each water oxygen atom (for example, O7W-H7···O5 and O7W-H7'···O5') are symmetry equivalent.

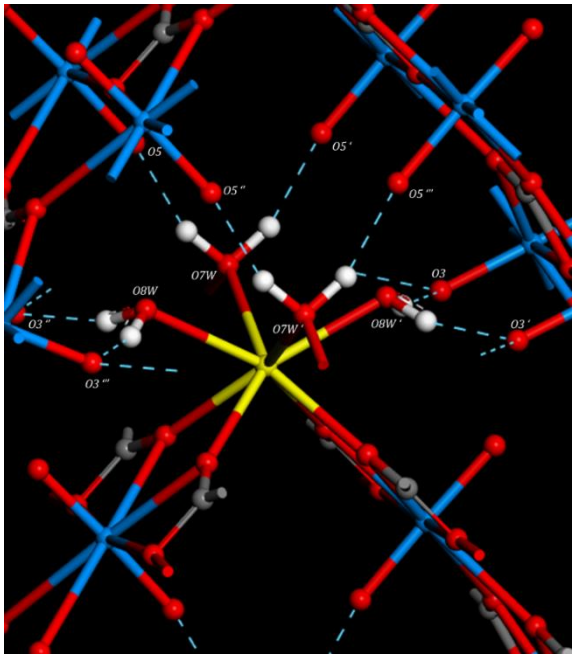

Fig. 7. Hydrogen bonding in the computed crystal structure of sharpite. Color code: U - Blue; Ca - Yellow; C- Gray; O - Red; H - White.

3.2.3.3 X-ray diffraction pattern

For sharpite, the X-ray diffraction patterns derived from the computed and experimental[83] structures (CuK_α radiation) are given in Fig. 3.C. The positions of the most intense reflections in the theoretical and experimental patterns are given in Table S.11 of the ESI.† The differences are rather low, the largest deviation being $\Delta(2\theta) \sim 0.6°$ for the [2 0 0] reflection.

3.2.4 Widenmannite, $Pb_2[(UO_2)(CO_3)_2(OH)_2]$

3.2.4.1 Crystal Structure

Widenmannite, $Pb_2[(UO_2)(CO_3)_2(OH)_2$, was described for the first time by Walenta and Wimmenauer[75] in 1961 from one specimen originating in Michael Mine in Weiler, near Lahr, in the Black Forest, Germany. It was named after Johann Friedrich Wilhelm Widenmann, a German mining official who first reported on the occurrence of a uranium mica in the Black Forest in 1793. It was also found in 1995 during a study of supergene uranium mineralization in the St. Just district of West Penwith, Cornwall, England by Elton and Hooper,[93] where it occurs in a localized patch of a Pb-U-Cu mineralization zone. Widenmannite was identified utilizing X-ray diffraction and energy dispersive X-ray analysis. Compositional and infrared spectroscopic studies were also performed.[93] However, the formula given for widenmannite, $Pb_2[(UO_2)(CO_3)_2]$ was not entirely correct. Widenmannite was later also found in several localities from the Czech Republic,[84-85] Finland[168] and USA.[169]

The crystal structure of widenmannite has been refined only in one occasion,[85] using precession electron-diffraction and synchrotron powder-diffraction methods due to the fact that widenmannite forms fine-grained poorly crystalline aggregates that yield X-ray powder diffraction patterns of insufficient quality for full structure refinement. The nature of widenmannite afforded by the work by Plášil *et al*.[85] was radically different to that from all previous studies. This works established that widenmannite lead uranyl carbonate mineral is not a tricarbonate as was previously believed.[85] Since the structure has been determined so far only in this single study, the optimization of the crystal structure using first principles solid-state methods provides an excellent opportunity for confirming its structure. The optimization was performed for an idealized structure because the true one was shown to contain a partially occupied site for uranium atom. The description of the complete structure, including the small occupation of this site, leads to an extremely complicated supercell structure whose optimization was not carried out. Even so, it was observed that the first principles geometrical optimization involving the idealized structure leads to unit-cell parameters, structural properties and X-ray diffraction patterns in satisfactory agreement with experiment, thus confirming the crystal structure reported by Plášil *et al*.[85]

The computed crystal structure of widenmannite is shown in Fig. 8. There is only one symmetry independent uranium atom displaying hexagonal bipyramidal coordination in the idealized crystal structure of widenmannite. The unit cell also comprises two non-equivalent carbon atoms (C1 and C2), which are surrounded by three oxygen atoms forming planar triangular

carbonate units. Finally, the unit cell contains a single non-equivalent lead atom. Setting the cutoff for the Pb-O bond length to 3.5 Å, the lead atom displays a coordination number of eleven. The form of the resulting coordination polyhedron, shown in Fig. 8.D, is determined to a large extent by the presence of lone electron pair in Pb^{2+} cation, which causes the existence of a large plane face in the polyhedron. The set of lead atom ligands includes eight oxygen atoms and three hydroxyl ions, $PbO_8(OH)_3$.

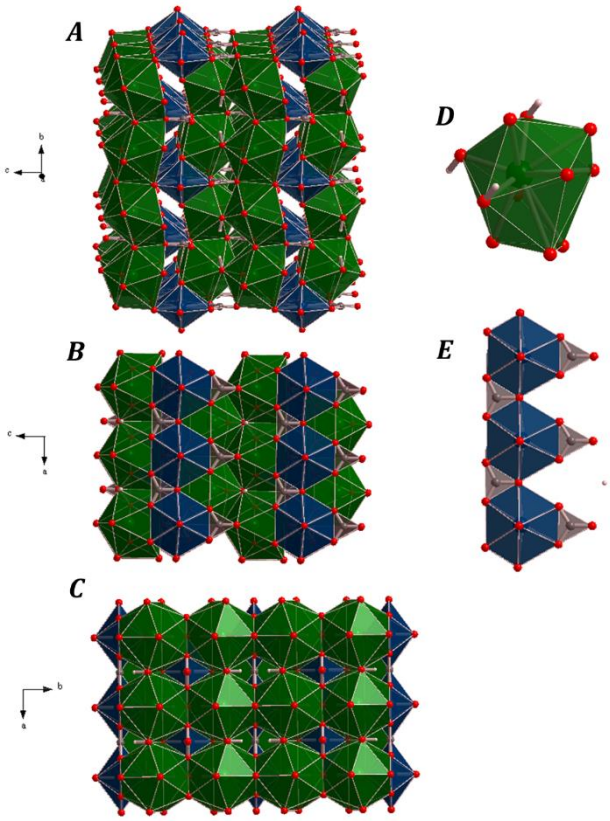

Fig. 8. Computed crystal structure of widenmannite. (A) View of a 2 × 2 × 2 supercell from [100]; (B) View of a 2 × 2 × 2 supercell from [010]; (C) View of a 2 × 2 × 2 supercell from [001]; (D) Lead coordination polyhedron; (E) Uranyl carbonate chain in widenmannite. Color code: U - Blue; Pb - Green; C - Gray; O - Red; H - White.

The crystal structure of widenmannite consists of corner-sharing uranyl hexagonal bipyramids, forming infinite chains expanding along [100], as shown in Fig. 8.E. From this figure, it is an easy matter to visualize these chains within the crystal structure, for example, in Fig. 8.B. The left triangular space between the two adjacent bipyramids is filled with a carbon atom which forms a C1 carbonate triangle. In addition, carbon atoms are bonded to two equatorial oxygen atoms of an edge of the bipyramid and to an oxygen atom of the lead coordination polyhedra forming a C2 carbonate triangle. The combination of the chains with the carbonate triangles results in the formation of the widenmannite uranyl carbonate chains, displayed in Fig. 8.E, which are not present in the structure of any other known uranyl carbonate mineral. The framework structure of widenmannite is formed from the uranyl carbonate chains which are connected *via* the lead coordination polyhedra. In turn, the lead polyhedra are interconnected forming ribbons parallel to [010]. These ribbons are linked by sharing one vertex of each lead polyhedra forming a layer parallel to (001) plane, as shown in Fig. 8.C.

The interatomic distances and angles obtained from the computed structure are compared with the experimental ones in Tables S.12 and S.13 of the ESI.† The experimental and computed average apical U-O distances are 1.80(2) and 1.784 Å. Likewise, the experimental and computed average equatorial U-O distances, 2.46(3) and 2.472 Å , are also in good agreement. The agreement between the experimental and calculated average Pb-O distances, 2.93(4) and 2.942 Å, is excellent. Finally, the experimental average C1-O and C2-O distances, 1.29(4) and 1.31(4) Å, agree satisfactorily with the computed values, 1.292 and 1.294 Å, respectively.

3.2.4.2 Hydrogen bonding

There are two non-equivalent hydrogen bonds in the crystal structure of widenmannite. They are O6-H1···O2 and O6-H1'···O4 and are clearly shown in Fig. 9. In both hydrogen bonds, the donor oxygen atom is the hydroxyl oxygen O6 belonging to the coordination polyhedra of Pb atom and the acceptor oxygens (O2 and O4) are equatorial oxygens from the uranyl hexagonal bipyramids. Therefore, the hydrogen bonds in widenmannite have the primary function of reinforcing the link between the uranyl carbonate chains and lead ribbons. The computed hydrogen bond parameters are given in Tables S.12 and S.13. The hydrogen bond O6-H1'···O4 should be quite weak due to the large value of the H1'···O4 distance and the small hydrogen bond angle.

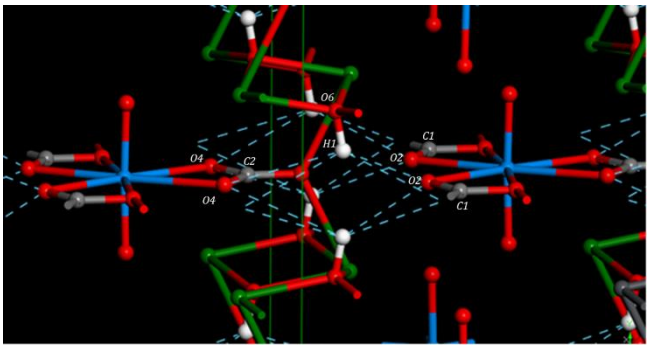

Fig. 9. Hydrogen bonding in the computed crystal structure of widenmannite. In the image, many Pb-O bonds have been deleted to show the hydrogen bond network in a better way. Color code: U - Blue; Pb - Green; C - Gray; O - Red; H - White.

3.2.4.3 X-ray diffraction pattern

The positions of the most intense reflections in the theoretical and experimental X-ray diffraction patterns of widenmannite (CuK_α radiation) are given in Table S.14 of the ESI.† The differences between these positions are quite small, the largest deviation being $\Delta(2\theta) \sim 0.7°$ for the [0 4 0] reflection.

3.2.5 Grimselite, $K_3Na[(UO_2)(CO_3)_3] \cdot H_2O$

3.2.5.1 Crystal Structure

A synthetic material with composition $K_3Na[(UO_2)(CO_3)_3]$ was described by Mazzi and Rinaldi[92] in 1962. However, the corresponding natural material, the mineral grimselite, was found eleven years later by Walenta.[77] The natural mineral was found in the Aar massif, Grimsel area, Bern, Switzerland. Thus, the name of the mineral refers to the locality in which it was encountered for the first time. It contains one water molecule per formula unit, $K_3Na[(UO_2)(CO_3)_3] \cdot H_2O$ and, therefore, it was believed that it was slightly different to the material synthetized by Mazi and Rinaldi,[92] even although the same hexagonal space symmetry, $P\bar{6}2c$, and lattice parameters were proposed. Grimselite was subsequently described from Krunkelbachtal, Germany[170] and Jáchymov, Czech Republic.[171] The synthetic analogue of grimselite was obtained again by Li and Burns[79] in 2001 and, in this case, the presence of water in its unit cell was reported. The crystal structure of the synthetic analogue of grimselite was studied by Li and Burns[79] which reported also hexagonal space symmetry ($P\bar{6}2c$). The structure of the rubidium synthetic analogue of grimselite was subsequently determined by Kubatko and Burns[172] in 2004. Thermodynamic and solubility data for grimselite have been published.[3b,15-16] Although the crystal structures reported up to date for grimselite are consistent,[79,86] the determination of the positions of the hydrogen atoms in the unit cell of grimselite has not been possible so far and are obtained in this work using theoretical methods. It must be noted that, according to the present calculations, although the space symmetry of the unit cell of grimselite without the hydrogen atoms is hexagonal, the space symmetry becomes triclinic ($P1$) when the hydrogen atoms are included.

The computed crystal structure of grimselite is shown in Fig. 10. It contains a single symmetrically unique uranium atom displaying uranyl hexagonal bipyramidal coordination. It also contains one symmetrically unique carbon atom and two symmetrically distinct monovalent atoms, potassium and sodium. Carbon shows the usual planar triangular coordination. Sodium is coordinated by eight oxygen atoms located at the vertices of a hexagonal bipyramid (Fig. 10.E). The potassium atom is coordinated by eight oxygen atoms and one water molecule (Fig. 10.F). There is only one water molecule per formula unit, which will be denoted as W5. The position of the water oxygen atom is partially filled with an occupation of 50%. The crystal structure of grimselite contains uranyl tricarbonate groups (Fig. 10.D) sharing one edge of each carbonate triangle with a different sodium hexagonal bipyramid (Fig. 10.B). The tricarbonate groups and the sodium polyhedra form heteropolyhedral layers parallel to plane (001), as shown in Fig. 10.B. The layers are held together by sharing the apical vertices of the uranium and sodium bipyramids of two adjacent layers (Fig. 10.C). The voids in the heteropolyhedral layers contain potassium coordination polyhedral, which include the water molecules and strengthen the connection between the layers.

The bond distances derived from the calculated crystal structure of grimselite are compared with the experimental[86] ones in Table S.15 of the ESI.† The experimental and computed average apical U-O distances are 1.785(8) and 1.823 Å, respectively. Similarly, the experimental and computed average equatorial U-O distances are 2.418(8) and 2.434 Å. The agreement between the experimental and calculated average Na-O distances, 2.615(8) and 2.631 Å, and K-O distances, 2.826(9) and 2.817 Å, is satisfactory. Lastly, the experimental average C-O distance, 1.298(2) Å, is in good agreement with the computed value of 1.297 Å.

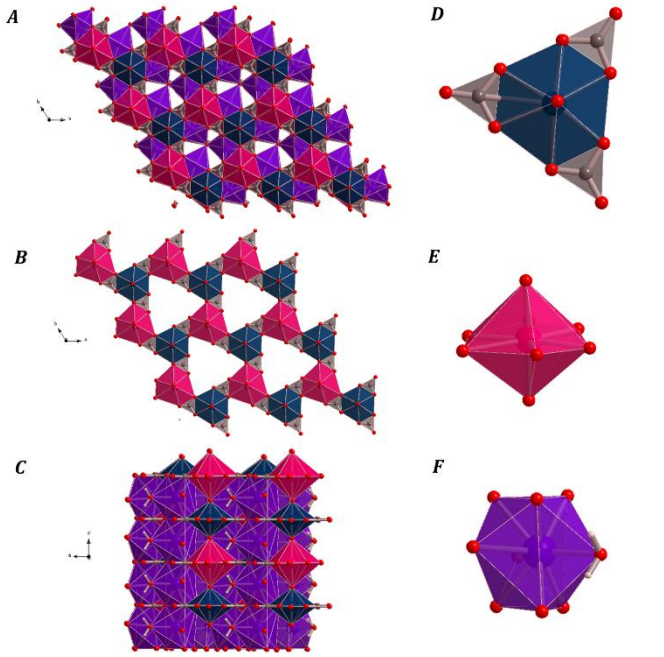

Fig. 10. Computed crystal structure of grimselite: (A) View of a 3 × 3 × 3 supercell from [001]; (B) Structural layer formed by uranyl tricarbonate layers linked by sodium hexagonal bipyramids; (C) View of a 2 × 2 × 2 supercell from [010] showing the connection between the sodium uranyl tricarbonate layers; (D) Uranyl tricarbonate group; (E) Sodium hexagonal bipyramid coordination polyhedron; (F) Potassium coordination polyhedron. Color code: U - Blue; K - Violet; Na - Pink; C -Gray; O - Red; H - White.

3.2.4.2 Hydrogen bonding

The hydrogen bonds in grimselite crystal structure are shown in Fig. 11. There is only one water molecule per formula unit in grimselite and only two non-equivalent hydrogen bonds. The computed hydrogen bond parameters are given in Table S.16 of the ESI.† These hydrogen bonds link the potassium coordination polyhedra with the carbonate triangles and, therefore, serve to reinforce the linkage between two successive heteropolyhedral sheets.

3.2.5.3 X-ray diffraction pattern

The positions of the most intense reflections in the theoretical and experimental X-ray diffraction patterns of widenmannite (CuK_α radiation) are given in Table S.15 of the ESI.† The most significant deviation between the computed and experimental positions is $\Delta(2\theta) \sim 0.5°$ for the [3 1 2] reflection.

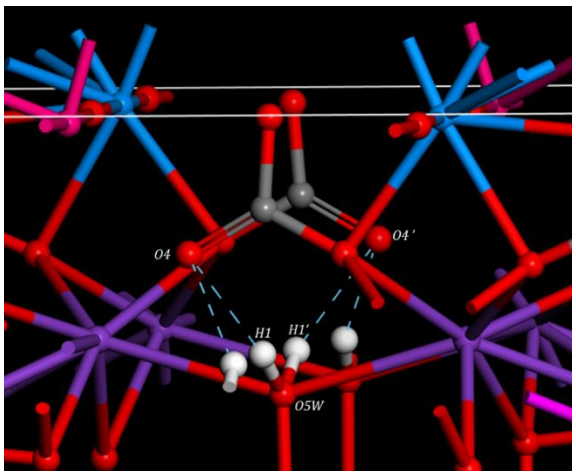

Fig. 11. Hydrogen bonding in the computed crystal structure of grimselite. Color code: U - Blue; K - Violet; Na - Pink; C - Gray; O - Red; H - White.

3.2.6 Čejkaite, $Na_4[(UO_2)(CO_3)_3]$

3.2.6.1 Crystal Structure

Čejkaite mineral was described for the first time as a new mineral by Ondruš *et al.*[88] in 2003, although its synthetic trigonal analogue was already studied in 2001.[80,87] The first mineral sample of čejkaite was found in Jáchymov, Western Bohemia, Czech Republic. Its name was chosen in honor of Jiří Čejka, for his outstanding contributions to the knowledge of uranium minerals and their spectroscopy. Čejkaite has been encountered at several localities worldwide as Rožná, Western Moravia, Czech Republic[173] and in Mina Euréka, Pyrenees, Spain.[174-175] Čejkaite was also found in sediments at the Hanford site, where it resulted from uranium soil contamination.[58-59] It was also encountered as a weathering product on the surface of the Chernobyl lava.[53]

The definitive monoclinic space symmetry and crystal structure of čejkaite was established in 2013 by Plášil *et al*.[90] from single-crystal X-ray diffraction data collected from a natural twinned microcrystal. In the previous studies,[80,87-88] a triclinic unit cell had been reported. Catalano and Brown[176] in 2004 provided information about the bond lengths in the uranium coordination polyhedron in čejkaite from the analysis of its EXAFS spectrum, and Čejka *et al.*[89] in 2010 reported the Raman spectrum for čejkaite.

There is one symmetrically independent uranium atom (U), three non-equivalent carbon atoms (C1, C2 and C3) and four sodium atoms (Na1, Na2, Na3 and Na4) in the unit cell of čejkaite.[90] The uranium atom display uranyl hexagonal bipyramidal coordination. Three equatorial edges of the uranyl bipyramid are shared with three planar carbonate triangles (associated with C1, C2 and C3), as shown in Figs. 12.A and 12.C. Thus, as grimselite, čejkaite is an uranyl tricarbonate mineral. The equatorial plane of the uranyl tricarbonate groups are perpendicular to [001]. The sodium atoms are coordinated by six oxygen atoms forming highly distorted octahedra. The sodium polyhedra of Na2, Na3 and Na4 share one of its edges with the equatorial edges of uranium bipyramids which are not shared with the carbonate triangles, forming trigonal sodium uranyl tricarbonate units, as shown in Fig. 12.C. The sodium octahedra also share one of its vertices with Na1 polyhedra (see Fig. 12.A). The sodium octahedra associated with Na1 atoms share two opposite faces with two other Na1 octahedra leading to the formation of chains (or columns) arranged in the direction perpendicular to the plane of sodium uranyl tricarbonate units ([001]). These columns are shown in Figs. 12.B and 12.D. From the sodium uranyl tricarbonate units and Na1 octahedra, complicated sodium uranyl-carbonate sheets, parallel to (001) plane, are formed in čejkaite as shown in Fig. 12.E.

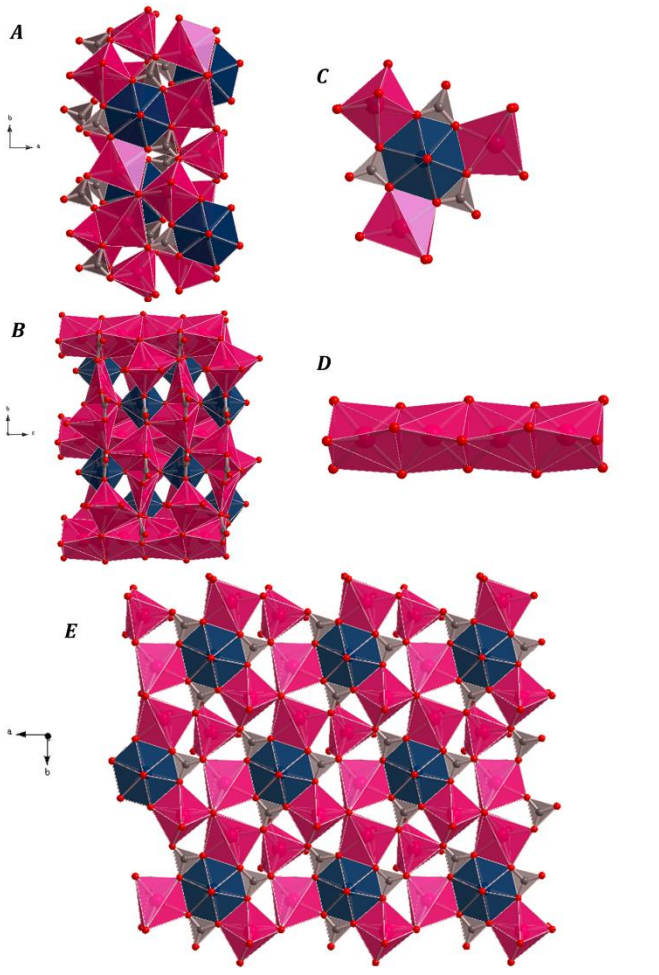

Fig. 12. Calculated crystal structure of čejkaite . (A) View of the unit cell from [001]; (B) View of the unit cell from [100]; (C) A sodium uranyl tricarbonate group; (D) A Na1 column; (E) A sodium uranyl tricarbonate layer. Color code: U - Blue; Na - Pink; C - Gray; O - Red.

Journal Name

ARTICLE

Table 2. Computed elastic constants of selected uranyl carbonate minerals. All the values are given in GPa.

ij	C_{ij}							
	Roubaultite	Fontanite	Sharpite	Widenmannite	Grimselite	Čejkaite	Rutherfordine[124]	Bayleyite[101]
11	125.33	92.00	197.71	123.46	66.50	106.37	272.60	32.08
22	49.34	39.98	55.34	63.67	60.72	112.18	22.69	49.05
33	59.10	1.43	48.82	63.31	55.36	47.01	178.07	46.91
44	30.52	6.57	18.17	4.08	18.95	14.05	6.08	11.59
55	16.38	20.20	0.54	10.99	19.28	16.58	66.90	11.35
66	18.08	1.82	28.33	1.26	29.80	53.73	9.87	9.66
12	30.08	6.04	-11.29	26.23	21.56	53.09	-7.61	20.95
13	22.26	-5.27	-9.60	19.92	19.52	9.70	77.03	21.12
14	2.25	0.0	0.0	0.0	0.68	0.0	0.0	0.0
15	12.82	-2.82	0.0	0.0	0.05	-4.29	0.0	-2.43
16	6.59	0.0	0.0	0.0	1.15	0.0	0.0	0.0
23	27.68	14.32	25.95	16.10	18.83	9.35	-6.12	29.21
24	6.04	0.0	0.0	0.0	0.83	0.0	0.0	0.0
25	11.26	-0.72	0.0	0.0	-0.02	-2.24	0.0	-1.07
26	2.84	0.0	0.0	0.0	-2.39	0.0	0.0	0.0
34	13.69	0.0	0.0	0.0	1.52	0.0	0.0	0.0
35	7.20	-7.14	0.0	0.0	-0.33	-4.41	0.0	-0.65
36	5.97	0.0	0.0	0.0	-0.70	0.0	0.0	0.0
45	10.09	0.0	0.0	0.0	-0.54	0.0	0.0	0.0
46	5.39	-1.60	0.0	0.0	0.00	-1.45	0.0	-1.80
56	14.33	0.0	0.0	0.0	0.01	0.0	0.0	0.0

Table S.18 of the ESI† provides the most important computed interatomic distances between the atoms in the unit cell of čejkaite. The comparison of the experimental and computed average apical U-O distances, 1.86 and 1.840 Å, is quite satisfactory. The computed experimental and computed average equatorial U-O distances are 2.42 and 2.385 Å, respectively. The agreement between the experimental and computed Na-O distances for Na1, Na2, Na3 and Na4 is very good. The experimental values are 2.48, 2.39, 2.47 and 2.48 Å, and the calculated ones are 2.485, 2.448, 2.485 and 2.468 Å, respectively. The more significant difference is found for the Na2 octahedra, 0.06 Å, but for the Na1, Na3 and Na4 octahedra the differences are lower than 0.02 Å. Finally, the differences in the average C-O distances for the C1, C2 and C3 carbon atoms are smaller than 0.02 Å.

3.2.6.2 X-ray diffraction pattern

The positions of the most important reflections in the theoretical and experimental X-ray diffraction patterns of čejkaite (obtained using CuK_α radiation) are provided in Table S.19 of the ESI.† The larger difference between the computed and experimental positions is $\Delta(2\theta) \sim 0.5°$ for the [0 0 4] reflection.

3.3 Mechanical properties

3.3.1 Elasticity tensors and mechanical stability

The elasticity tensors of the six uranyl carbonates considered were computed at the corresponding energy-optimized crystal structures described in Section. 3.2. The elements of the matrix representations of the elasticity tensors, also known as elastic constants, are given in Table 2. In this table, the elastic constants of the rutherfordine and bayleyite uranyl carbonate minerals, determined in previous works,[124,101] have been also included. In Table 2, the indices of the matrix elements of the elasticity tensor are expressed employing Voigt convention in which a pair of Cartesian indices are contracted into a single integer (C_{ij} ;$1 \le i,j \le 6$: xx→1, yy→2, zz→3, yz→4, xz→5, xy→6). The space-group symmetry of a given crystalline material determines the number of non-vanishing elements in its elasticity matrix, which are not related by symmetry.[156,177] Since sharpite, widenmannite and rutherfordine have orthorhombic symmetry, their elasticity matrices have only nine non-vanishing and symmetry-independent elements. For fontanite, čejkaite and bayleyite, with monoclinic symmetry, the elasticity matrix has thirteen non-vanishing elements. Finally, for roubaultite and grimselite, all the matrix elements are non-vanishing (triclinic symmetry).

In order to investigate the mechanical stability of the crystal structures of the uranyl carbonate minerals studied, the satisfaction of the generic Born mechanical stability condition was studied. The necessary and sufficient generic Born condition[177-178] for mechanical stability of a given structure is that its elasticity matrix, C, must be positive definite, *i.e.*, all its eigenvalues must be positive. All the elasticity matrices given in Table 2 were diagonalized numerically. All the eigenvalues of the elasticity matrices for the six minerals were seen to be positive and, therefore, they are mechanically stable.

Journal Name

ARTICLE

Table 3. Computed mechanical properties of selected uranyl carbonate minerals. The values of the bulk, shear and Young moduli (B, G and E) are given in in GPa).

	Property	Roubaultite	Fontanite	Sharpite	Widenmannite	Grimselite	Čejkaite	Rutherfordine[124]	Bayleyite[101]
$\boldsymbol{B}$	Bulk modulus	43.75	18.18	32.04	39.53	33.26	39.34	17.90	27.52
$\boldsymbol{G}$	Shear modulus	23.24	13.61	15.82	9.98	21.08	25.99	14.12	9.86
$\boldsymbol{E}$	Young modulus	59.24	32.67	40.76	27.62	55.20	63.89	33.53	26.43
$\boldsymbol{\nu}$	Poisson's ratio	0.42	0.20	0.29	0.38	0.24	0.23	0.19	0.34
$\boldsymbol{D}$	Ductility index	1.88	1.33	2.02	3.96	1.58	1.51	1.27	2.79
$\boldsymbol{H}$	Hardness index	3.01	3.56	1.40	1.46	3.98	5.28	4.13	0.70
$\boldsymbol{A^U}$	Universal anisotropy	19.63	2.57	54.64	14.13	0.18	2.08	13.28	0.32

Table 4. Computed bulk modulus and pressure derivatives derived from the 4-BM EOS. The values of the bulk modulus computed from the elastic constants are given in the last row of the table for comparison

Property	Roubaultite	Fontanite	Sharpite	Widenmannite	Grimselite	Čejkaite	Rutherfordine[124]	Bayleyite[101]
				EOS				
$\boldsymbol{B}$ $(\boldsymbol{GPa})$	42.67 ± 3.54	22.93 ± 1.12	26.80 ± 0.64	39.46 ± 0.82	32.22 ± 0.50	37.19 ± 0.55	19.03 ± 0.37	33.05 ± 0.81
$\boldsymbol{B'}$	1.39 ± 2.30	2.28 ± 0.89	5.86 ± 0.77	6.00 ± 0.89	2.08 ± 0.36	4.79 ± 0.49	15.34 ± 0.72	0.27 ± 0.77
$\boldsymbol{B''(GPa^{-1})}$	0.21 ± 0.38	-0.13 ± 0.20	-0.51 ± 0.45	0.08 ± 0.44	0.21 ± 0.06	-0.01 ± 0.18	-7.44 ± 1.32	0.01 ± 0.07
$\boldsymbol{\chi^2}$	0.088	0.017	0.004	0.002	0.002	0.002	0.003	0.003
				Elastic constants				
$\boldsymbol{B}$ $(\boldsymbol{GPa})$	43.75 ± 1.45	18.18 ± 8.94	32.04 ± 4.85	39.53 ± 0.60	33.26 ± 2.15	39.34 ± 2.68	17.90 ± 0.40	27.52 ± 0.67

3.3.2 Mechanical properties

The mechanical properties of polycrystalline aggregates of the uranyl carbonate minerals studied were determined in terms of the computed elastic constants employing the Voigt,[179] Reuss[180] and Hill[181] schemes. For roubaultite and fontanite, the Voigt approximation gave the best comparison between the computed bulk modulus and the single-crystal bulk modulus extracted from the 4-BM EOS (see Section 3.3.3). For sharpite, widenmannite and čejkaite, the Hill approach worked better and, finally, for grimselite, the Reuss approach gave the best results. The computed mechanical properties using these approximations are reported in Table 3. The mechanical properties obtained for rutherfordine and bayleyite in previous papers[124,101] are also included in Table 3. For these two minerals, the Reuss approach was found to be the best approach.[124,101]

From the data given in Table 3, it follows that roubaultite, sharpite, widenmannite and bayleyite are ductile minerals because the computed ductility index is larger than 1.75.[182-183] On the contrary side, fontanite, grimselite, čejkaite and rutherfordine are brittle (D < 1.75). According to the results, roubaultite, fontanite, grimselite, čejkaite and rutherfordine are minerals of intermediate hardness,[184] čejkaite being the harder one (H = 5.3). Sharpite, widenmannite and bayleyite are weak, with values of the Vickers hardness smaller than 1.5.

Roubaultite, sharpite, widenmannite and rutherfordine are very anisotropic minerals since the corresponding universal anisotropy indices[185] are extraordinarily large, the case of sharpite being the most extreme one, because A^U= 54.6. Fontanite and čejkaite have also quite large mechanical anisotropies, but the corresponding indices are much smaller (2.6 and 2.0, respectively). Grimselite and bayleyite have very small universal anisotropy indices, 0.2 and 0.4, respectively.

The large mechanical anisotropy of roubaultite, sharpite and rutherfordine[124] is a direct consequence of their layered crystal structures. The bonding strength along the direction perpendicular to the structural layers, which are held together by hydrogen bonding in roubaultite and sharpite and van der Waals forces in rutherfordine,[114,118,124] is much smaller than along the directions parallel to the plane of the layers and, therefore, these minerals are highly anisotropic. The case of fontanite, also displaying a layered crystal structure, is quite different because the uranyl carbonate sheets are directly bonded through covalent bonds between the interlayer calcium atoms and the uranyl apical oxygen atoms within the sheets. The same occurs in čejkaite, the bonding strength between the sodium uranyl-carbonate sheets being dominated by the presence of covalent bonds. The anisotropy of widenmannite is also substantial, although it has a framework crystal structure. However, again, the bonding strength along the y and z directions in widenmannite is much smaller than along x direction and, as a consequence, the value of the matrix element of the elasticity matrix, C_{11}, is more than two times those of C_{22} and C_{33} (see Table 2) For grimselite and bayleyite,[101] the bonding character along the three spatial directions (dominated by covalent and hydrogen bonding types in grimselite and bayleyite,[101] respectively) is analogous and, therefore, the diagonal elements of the elasticity matrix along the three directions, C_{ii} $(i = 1,2,3)$, have very similar values.

Journal Name

ARTICLE

3.3.2 Equations of state

The crystal structures of the six uranyl carbonate minerals were optimized under the effect of seventeen different external hydrostatic pressures with values between -1.0 and 9.0 GPa. The obtained unit cell volumes and the corresponding pressures were then fitted to a 4-BM EOS[164-166]

$$P = 3\,B\,f_E\,(1+2f_E)^{\frac{5}{2}}\left[1+\frac{3}{2}(B'-4)f_E + \frac{3}{2}\left\{B\,B'' + (B'-4)(B'-3)\frac{35}{9}\right\}{f_E}^2\right] \quad (1)$$

where:

$$f_E = \frac{1}{2}\left[\left(\frac{V_0}{V}\right)^{\frac{2}{3}} - 1\right] \quad (2)$$

In Eq. (1) the fitting parameters (B, B' and B'') are the bulk modulus and its first and second derivatives with respect to pressure. The values obtained for these parameters are collected in Table 4. In all the cases, the bulk moduli obtained from the 4-BM EOS and from the calculated elastic constants are in satisfactory agreement.

3.3.3 Negative mechanical phenomena

Due to the strong correlation between the values of the universal anisotropy index and the difference of the values of the minimum and maximum Poisson's ratios when all possible directions of the applied strain are considered,[186,163] roubaultite, sharpite, widenmannite and rutherfordine, are firm candidates to show negative values of the Poisson's ratio, *i.e.*, to display the negative Poisson's ratio (NPR) phenomenon.[133-134] Fontanite and čejkaite are also good candidates since $A^U \sim 2$. Furthermore, it has been observed[158-162] that the presence of negative Poisson's ratios is frequently accompanied by the important negative linear compressibility (NLC) phenomenon.[135-136] Therefore, the dependence of the mechanical properties of these minerals on the orientation of the applied strain was studied explicitly to analyze the possible presence of negative mechanical phenomena.

No mechanical anomalies were found for grimselite, čejkaite and bayleyite. The mechanical behavior of bayleyite was already studied in a previous work.[101] The dependence of the compressibility (the inverse of the bulk modulus), Young and shear modulus and Poisson's ratio of grimselite and čejkaite on the orientation of the applied strain is shown in the lower part of Fig. 13. Two-dimensional projections of the tridimensional representations of the elastic properties provided in Fig. 13 are given in Figs. S.1 to S.8 of the ESI.† As expected from the very low mechanical anisotropy of grimselite, the directional dependence observed in Fig. 13 is very low. For čejkaite, the mechanical properties are only slightly more dependent on the orientation than in grimselite, as was anticipated by the larger universal anisotropy index, but no mechanical anomalies are observed.

As can be observed in Fig. 13, sharpite and widenmannite, display the NPR phenomenon. The minimum values of the Poisson's ratios as well as the corresponding directions of the applied strain are given in Table 5. The absolute value of the minimum Poisson's ratio in sharpite is extremely large, 1.72, in line with the large value of the computed value of the universal anisotropy index. The NPR effect in widenmannite is much less significant, the value of the minimum Poisson's ratio being $\nu_{min} = -0.21$. However, for sharpite and widenmannite, negative values of the compressibility are not observed. The mechanical behavior of rutherfordine mineral was shown to be very similar in a previous work.[124] The minimum Poisson's ratio in rutherfordine was close to that of widenmannite -0.27.

For roubaultite and fontanite, a highly anomalous mechanical behavior was found. Roubaultite displays the NPR phenomenon, the value of the minimum Poisson's ratio being, as in the case of sharpite, very significant ($\nu_{min} = -1.73$). Fontanite does not display negative Poisson's ratios. However, as shown in Fig. 14, both minerals exhibit negative values of the compressibility for a wide range of orientations of the applied strain. The directions of minimum compressibility for roubaultite and fontanite are (0.71, -0.28, 0.64) and (0.00, 0.00, 1.00), respectively.

Table 5. Minimum values of the Poisson's ratios in roubaultite, sharpite, widenmannite and rutherfordine. The directions for the associated longitudinal and transverse directions are also given

ν_{min}	U^L_{min}	U^T_{min}
Roubaultite		
-1.73	(0.17, 0.70, 0.69)	(0.73, 0.38, -0.57)
Sharpite		
-1.72	(0.28, 0.90, -0.34)	(-0.67, 0.44, 0.60)
Widenmannite		
-0.21	(0.48, 0.27, 0.83)	(0.59, 0.60, -0.54)
Rutherfordine[124]		
-0.27	(1.00, 0.00, 0.00)	(0.00, 1.00, 0.00).

Journal Name

ARTICLE

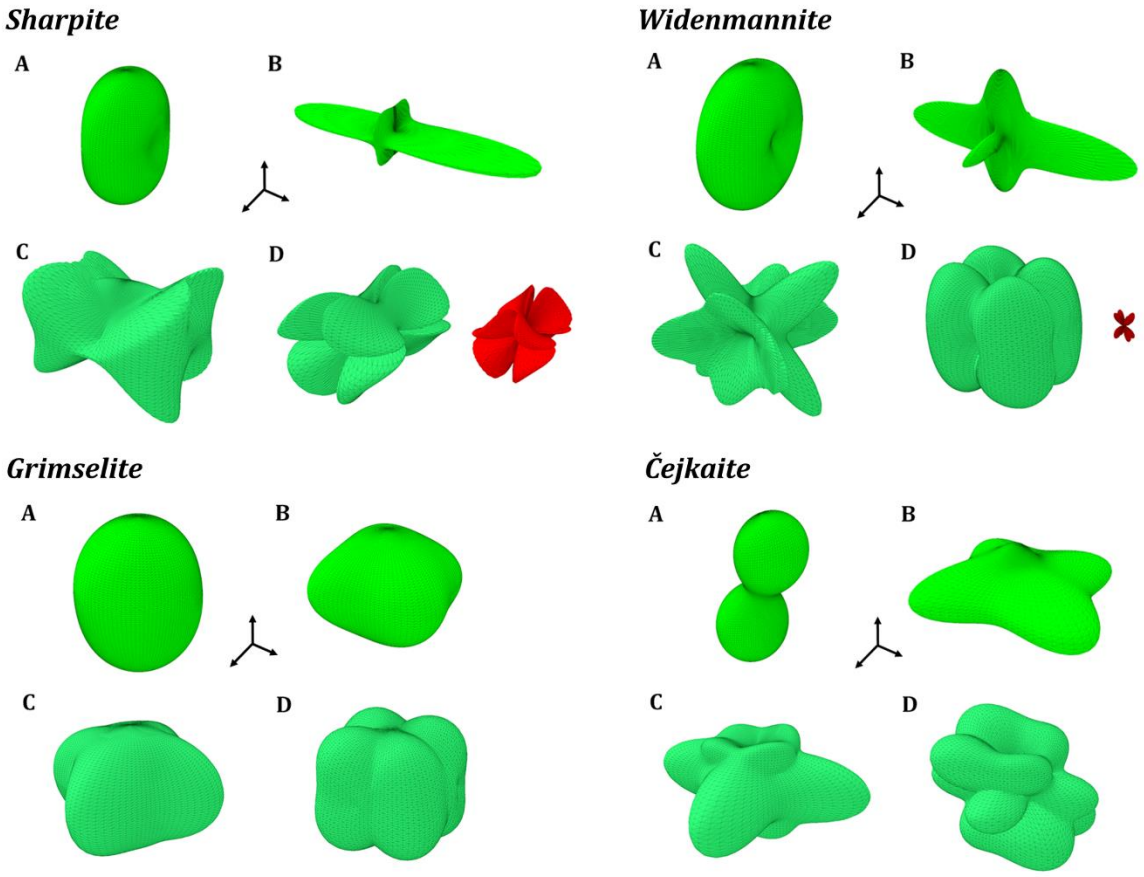

Fig. 13. Elastic properties of sharpite, widenmannite, grimselite and čejkaite as a function of the orientation of the applied strain: (A) Compressibility; (B) Young modulus; (C) Maximum shear modulus; (D) Maximum Poisson's ratio. For sharpite and widenmannite, displaying the NPR phenomenon, the surface of minimum Poisson's ratio is also shown (red surface). The maximum values of the compressibility, Young modulus, shear modulus and Poisson's ratio are: (A) Sharpite: 15.25 TPa^{-1}, 194.91 GPa, 41.79 GPa and 2.43; (B) Widenmannite: 11.75 TPa^{-1}, 109.67 GPa, 32.72 GPa and 1.06; (C) Grimselite: 12.12 TPa^{-1}, 65.96 GPa, 30.14 GPa and 0.35; (D) Čejkaite: 20.76 TPa^{-1}, 128.26 GPa, 53.78 GPa and 0.52.

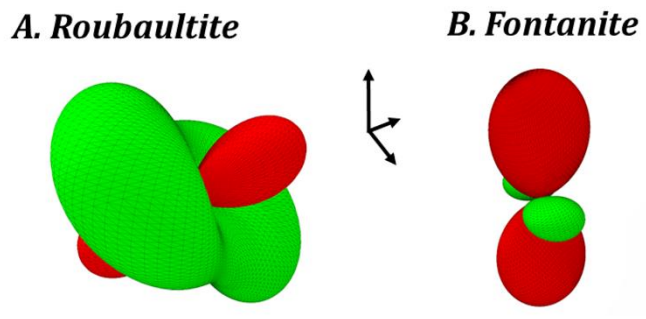

Fig. 14. The compressibility of roubaultite and fontanite as a function of the orientation of the applied strain. The positive and negative values of the compressibility are plotted in green and red, respectively. The maximal values of the compressibility for roubaultite and fontanite are 45.88 and 62.60 TPa^{-1}, respectively.

3.3.3.1 The anisotropic NLC effect in roubaultite

The unit cell of roubaultite was optimized under the effect of nine different anisotropic external pressures applied along the minimum compressibility direction. The computed unit-cell volumes, unit cell parameters and compressibilities are given in Tables S.20 and S.21 of the ESI.† The computed unit cell volumes and compressibilities are plotted as a function of the applied pressure in Fig. 15. As may be observed, the unit cell volumes increase for anisotropic pressures in the range from −0.023 to −0.014 GPa and, therefore, the volumetric compressibility, $k_V = -1/V \cdot (\partial V/\partial P)_P$ is negative in this pressure range. Thus, roubaultite displays the anisotropic NLC (ANLC) phenomenon.[160-162] The compressibility is minimum at P = −0.017 GPa, k_V=−33.96 TPa^{-1}.

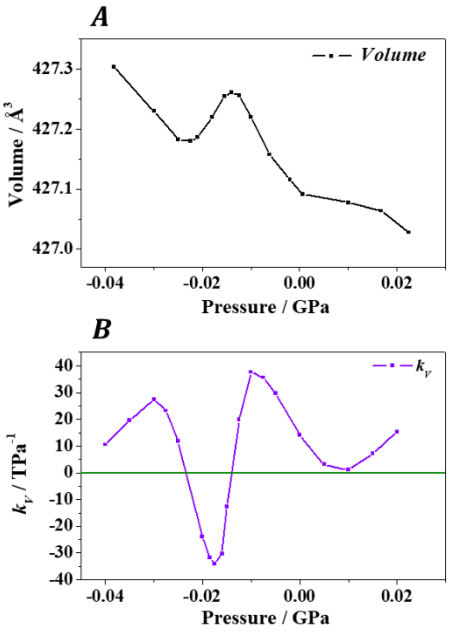

Fig. 15. Unit cell volumes and compressibilities ($k_V = -1/V \cdot (\partial V/\partial P)_P$) of roubaultite under the effect of different external pressures applied along the direction of minimum compressibility.

3.3.3.2 The anisotropic NLC effect in fontanite

The crystal structure of fontanite mineral was optimized under the effect of ten different anisotropic external pressures applied along the minimum compressibility direction, which in this case coincides with the [001] crystallographic direction. An increased plane wave kinetic energy cutoff of 1000 eV was employed in the calculations. The computed unit-cell volumes, unit cell parameters and compressibilities as a function of the applied external pressure are given in Tables S.22 and S.23 of the ESI,† and are plotted in Fig. 16. The unit-cell volume and parameters of fontanite show a large variation for an applied pressure near zero pressure (P ~ 0.001 GPa). The unit-cell volume increases by about 0.8% (~ 15.5 Å^3) at this pressure. While the variations that are shown in Fig. 16 may seem to correspond to a structural phase transition, a plot of the crystal structures at the pressures P = −0.015 GPa and P = 0.019 GPa, given in Fig. S.9 of the ESI,† demonstrates that no topological changes in the bond structure of fontanite are produced by the application of small anisotropic pressures directed along the direction of minimum compressibility, although significant variations of the dimensions of the unit cell are observed.

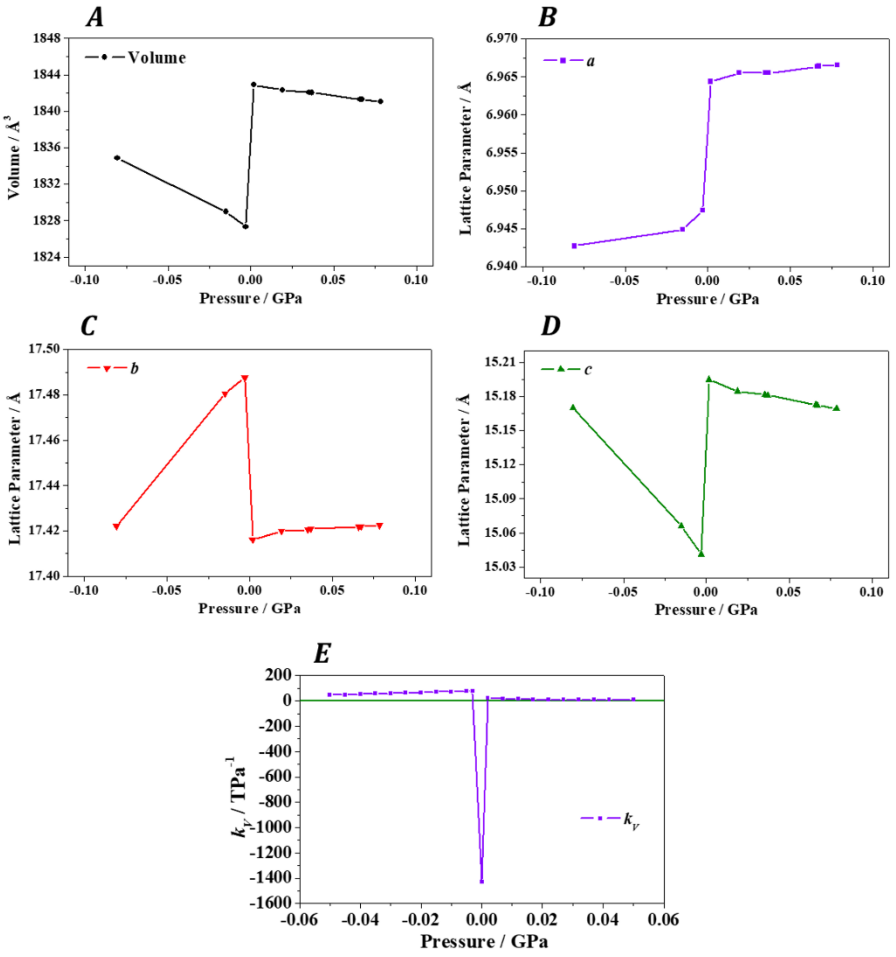

Fig. 16. Unit cell volumes, lattice parameters and compressibilities ($k_V = -1/V \cdot (\partial V/\partial P)_P$) of fontanite under the effect of different external pressures applied along the direction of minimum compressibility.

3.3.3.3 The isotropic NLC effect in sharpite

The study of the dependence of the mechanical properties of a given material on the orientation of the applied strain does not allow to recognize the presence of mechanical anomalies when the material is submitted to isotropic (or hydrostatic) pressures (uniform in all directions). Therefore, the optimized crystal structures obtained for the determination of the equations of state of the uranyl carbonate minerals studied in this paper (see Section 3.3.2), corresponding to these materials under the effect of a large number of isotropic pressures, were examined. The analysis showed that, with the exception of sharpite, all the uranyl carbonate minerals display a normal mechanical behavior under isotropic pressure, *i.e.*, all the unit cell parameters decrease invariably under isotropic compression. However, for sharpite, as shown in Fig. 17, the a lattice parameter increases from P = 0.023 GPa and P = 0.299 GPa. Therefore, sharpite exhibits the isotropic NLC (INLC) effect[135-136,158-162] in this pressure range. The computed unit cell volumes, parameters and compressibilities are given in Tables S.24 and S.25 of the ESI.† The compressibility along a direction ($k_a = -1/a \cdot (\partial a/\partial P)_P$), is minimum at 0.185 GPa, $k_a = -22.32$ TPa^{-1}.

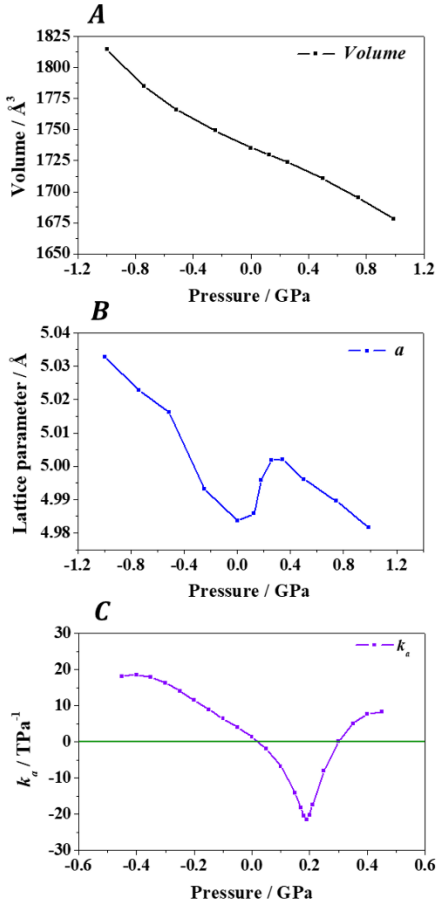

Fig. 17. Unit cell volumes, $\boldsymbol{a}$ lattice parameters and compressibilities ($\boldsymbol{k_a = -1/a \cdot (\partial a/\partial P)_P}$) of sharpite under the effect of different external isotropic pressures.

4 Conclusions

In this paper, the full crystal structures of the uranyl carbonate minerals fontanite, sharpite and grimselite, are determined for the first time using first principles solid-state methods based in Density Functional theory. This work is essential since the determination of the positions of the hydrogen atoms in their unit cells has not been possible so far due to the poor quality of their X-ray diffraction patterns. The energy-optimized crystal structures of the roubaultite, widenmannite and čejkaite minerals are also determined. The computed unit cell parameters and interatomic distances and angles are in good agreement with the available experimental information for the six minerals. Furthermore, the X-ray diffraction patterns are also consistent with the experimental patterns. The hydrogen bonding network present in the unit cells of the fontanite, sharpite and grimselite minerals are described in detail.

The availability of the energy-optimized crystal structures of these important uranyl carbonate minerals allowed for the determination of the elastic tensors and equations of state of these minerals using the first principles methodology. From them, an extended set of mechanical properties of these minerals were computed. This set includes the bulk, Young and shear moduli, the Poisson's ratio, ductility, hardness and anisotropy indices and the first two derivatives of the bulk modulus with respect to pressure. Four of these minerals, roubaultite, fontanite, sharpite and widenmannite, are shown to have very large mechanical anisotropies and to exhibit anomalous negative mechanical phenomena under the effect of small external hydrostatic or anisotropic pressures. The knowledge of the full crystal structures of these minerals should allow for the determination of the vibrational spectra and additional physico-chemical properties of these minerals by using theoretical methods, providing new information relevant for their identification and for improving our understanding about the paragenetic sequence of uranium minerals arising from the oxidative dissolution processes occurring in uranium ore deposits and from corrosion of spent nuclear fuel in nuclear waste repositories.

Conflict of Interest

There are no conflicts of interest to declare.

Acknowledgements

The supercomputer time provided by the CTI-CSIC center is greatly acknowledged. This work has been carried out in the context of a CSIC–CIEMAT collaboration agreement: "Caracterización experimental y teórica de fases secundarias y óxidos de uranio formados en condiciones de almacenamiento de combustible nuclear". JP acknowledges the support of the Czech Science Foundation through the project GACR 20-11949S. JS was supported by the Ministry of Culture of the Czech Republic (long-term project DKRVO 2019-2023/1.II.b; National Museum, 00023272).

References

1 D. L. Clark, D. E. Hobart, M. P. Neu, Actinide Carbonte Complexes and Their Importance in Actinide Environmental Chemistry, *Chem. Rev*., 1995, **95**, 25.

2 a) D. Langmuir, Uranium solution-mineral equilibria at low temperatures with applications to sedimentary ore deposits, *Geochim. Cosmochim. Acta*, 1978, **42**, 547; b) D. Langmuir, *Aqueous Environmental Geochemistry*, Prentice-Hall, New York, 1997; pp. 486−557.

3 a) A. K. Alwan, P. A. Williams, The aqueous chemistry of uranium minerals. Part 2. Minerals of the liebigite group, *Mineral. Mag*., 1980, **43**, 665; b) T. J. O'Brien, P. A. Williams, The aqueous chemistry of uranium minerals. 4. Schröckingerite, grimselite, and related alkali uranyl carbonates, *Mineral. Mag*., 1983, **47**, 69.

4 B. S. Hemingway, *Thermodynamic properties of selected uranium compounds and aqueous species at 298.15 K and 1 bar and at higher temperatures – Preliminary models for the origin of coffinite deposits*, USGS Open-File Report 82‑619, U.S. Geological Survey, 1982.

5 a) R. J. Finch, R. C. Ewing, *Uraninite alteration in an oxidizing environment and its relevance to the disposal of spent nuclear fuel*, SKB Technical Report 91-15, Swedish Nuclear Fuel and Waste Management Co, SKB, Stockholm, 1991; b) R. J. Finch, R. C. Ewing, The corrosion of uraninite under oxidizing conditions, *J. Nucl. Mater*., 1992, **190**, 133.

6 R. J. Finch, Thermodynamic stabilities of U(VI) minerals: Estimated and observed relationships, *Mat. Res. Soc. Symp. Proc*., 1997, **465**, 1185

7 R. J. Finch, T. Murakami, Systematics and Paragenesis of Uranium Minerals, *Rev. Mineral. Geochem*., 1999, **38**, 91.

8 a) D. J. Wronkiewicz, J. K. Bates, T. J. Gerding, E. Veleckis, B. S. Tani, Uranium Release and Secondary Phase Formation During Unsaturated Testing of UO_2 at 90 °C, *J. Nucl. Mater*., 1992, **190**, 107; b) D. J, Wronkiewicz, J. K. Bates, S. F. Wolf, E. C. Buck, Ten-Year Results from Unsaturated Drip Tests with UO_2 at 90 °C: Implications for the Corrosion of Spent Nuclear Fuel, *J. Nucl. Mater*., 1996, **238**, 78.

9 P. C. Burns, R. C Ewing, F. C Hawthorne, The crystal chemistry of hexavalent uranium; polyhedron geometries, bond-valence parameters, and polymerization of polyhedra, *Can. Mineral*.,1997, **35**, 1551.

10 a) P. C. Burns, The Crystal Chemistry of Uranium, *Rev. Mineral. Geochem*., 1999, **38**, 23; b) P. C. Burns, U^{6+} minerals and inorganic compounds: insights into an expanded structural hierarchy of crystal structures, *Can. Mineral*., 2005, **43**, 1839.

11 A. J. Lussier, R. A. K. Lopez, P.C. Burns, Revised and Expanded Structure Hierarchy of Natural and Synthetic Hexavalent Uranium Compounds, *Can. Mineral*., 2016, **54**, 177.

12 I. Grenthe, J. Fuger, R. J. M. Konings, R. J. Lemire, A. B. Muller, C. Nguyen-Trung, H. Wanner, *Chemical Thermodynamics of Uranium,* Nuclear Energy Agency Organisation for Economic Co-Operation and Development, OECD, Issy-les-Moulineaux, France, 2004.

13 N. Y. R. Guillaumont, T. Fanghänel, V. Neck, J. Fuger, D. A. Palmer, I. Grenthe, M. H. Rand, *Update on the Chemical Thermodynamics of Uranium, Neptunium, Plutonium, Americium, and Technetium*, ed. F. J. Mompean, M. Illemassene, C. Domenech-Orti, K. Ben Said, OECD Nuclear Energy Agency, Data Bank, Issy-les-Moulineaux, France, 2003.

14 I. Grenthe, J. Drozdzynski, T. Fujino, E. C. Buck, T. E. Albrecht-Schmitt, S. F. Wolf, Uranium, in *The Chemisty of Actinide and Transactinide Elements*, ed. L. R. Morss, N. M. Edelstein, J. Fuger, Springer Science and Business Media, Berlin, 2006; Chapter V, Vol. I; pp. 253–638.

15 K. A. Kubatko, K. B. Helean, A. Navrotsky, P. C. Burns, Thermodynamics of uranyl minerals: Enthalpies of formation of rutherfordine, UO_2CO_3, andersonite, $Na_2CaUO_2(CO_3)_3(H_2O)_5$, and grimselite, $K_3NaUO_2(CO_3)_3H_2O$, *Am. Mineral*., 2005, **90**, 1284.

16 D. Gorman-Lewis, P. C. Burns, J. B. Fein, Review of Uranyl Mineral Solubility Measurements, *J. Chem. Thermodyn*., 2008, **40**, 335.

17 S. V. Krivovichev, J. Plášil, Mineralogy and Crystallography of Uranium, in *Uranium: From Cradle to Grave*, ed. P. C. Burns, G. E. Sigmon, Mineralogical Association of Canada: Winnipeg, MB, Canada, 2013; Short Course 43; pp. 15–119.

18 J. Plášil, Oxidation-Hydration Weathering of Uraninite: The Current State of Knowledge, *J. Geosci*., 2014, **59**, 99.

19 R. J. Baker, Uranium Minerals and Their Relevance to Long Term Storage of Nuclear Fuels, *Coord. Chem. Rev*., 2014, **266–267**, 123.

20 M. S. Caceci, Environmental Chemistry of the Actinide Elements, in *Metal Speciation in the Environmen*t, ed. J. A. C. Broekaert, S. Gucer, F. Adams, NATO ASI Series (Series G: Ecological Sciences), Vol 23. Springer, Berlin, Heidelberg. 1990.

21 W. Runde, M. P. Neu, S. D. Reilly, Actinyl(VI) Carbonates in Concentrated Sodium Chloride Solutions: Characterization, Solubility, and Stability, in *Actinide Speciation in High Ionic Strength Media*, ed. D. T. Reed, S. B. Clark, L. Rao, Springer, Boston, MA, 1999.

22 K. Maher, J. R. Bargar, G. E. Brown, Environmental Speciation of Actinides, *Inorg. Chem*., 2013, **52**, 3510.

23 A. M. Giblin, B. D. Batts, D. J. Swaine, Laboratory simulation studies of uranium mobility in natural waters, *Geochim. Cosmochim. Acta*, 1981, **45**, 699.

24 S. Kojima, S. Takeda, S. Kogita, Chemical factors controlling the solubility of uraninite and their significance in the genesis of unconformity-related uranium deposits, *Mineral. Dep.*, 1994, **29**, 353.

25 H. M. Fernandes, L. H. S. Veiga, M. R. Franklin, V. C. S. Prado, J. F. Taddei, Environmental Impact Assessment of Uranium Mining and Milling Facilities; A Study Case at the Poços de Caldas Uranium Mining and Milling Site, Brazil, *J. Geochem. Expl*., 1996, **52**, 161.

26 S. Akhtara, X. Yanga, F. Pirajno, Sandstone type uranium deposits in the Ordos Basin, Northwest China: A case study and an overview, *J. Asian Earth Sci*., 2017, **146**, 367.

27 M. S. Colomina, A. Mangeret, L. Stetten, P. Merrot, O. Diez, A. Julien, E. Barker, A. Thouvenot, J. Bargar, C. Cazala, G. Morin, Carbonate Facilitated Mobilization of Uranium from Lacustrine Sediments under Anoxic Conditions, *Environ. Sci. Technol*., 2018, **52**, 9615.

28 B. Novotnik, W. Chen, R. D. Evans, Uranium Bearing Dissolved Organic Matter in the Porewaters of Uranium Contaminated Lake Sediments, *Appl. Geochem.*, 2018, **91**, 36.

29 S. E. Bone, J. Cliff, K. Weaver, C. J. Takacs S. Roycroft, S. Fendorf, J. R. Bargar, Complexation by Organic Matter Controls Uranium Mobility in Anoxic Sediments, *Environ. Sci. Technol*., 2020, **54**, 1493.

30 E. P. Bullwinkel, *The chemistry of uranium in carbonate solutions: Topical Report RMO-2614*, The Merrill Co., San Francisco, 1954.

31 C. A. Blake, C. F. Coleman, K. B. Brown, D. G. Hill, R. S. Lowrie, J. M. Schmitt, Studies in the Carbonate-Uranium System, *J. Am. Chem. Soc*., 1956, **78**, 5978.

32 a) I. I. Chernyaev, V. A. Golovnya, G. V. Ellert, Aqueous Carbonate Compounds of Uranyl, *Rus. J. Inorg. Chem*., 1956, **1**, 2726; b) A. K. Babko, V. S. Kodenskaya, Equilibria in solutions of uranyl carbonate complexes, *Rus. J. Inorg. Chem*., 1960, **5**, 1241.

33 a) E. I. Sergeyeva, A. A. Nikitin, I. L. Khodakovskiy , G. B. Naumov, Experimental investigation of equilibria in the system $UO_3 - CO_2 - H_20$ in 25-200 ℃ temperature interval, *Geokhimiya*, 1972, **11**, 1340; b) E. I. Sergeyeva, O. A. Devina, I. L. Khodakovsky, Thermodynamic database for actinide aqueous inorganic complexes, *J. Alloys Compd*., 1994, **213–214**, 125.

34 a) S. O. Cinnéide, J. P. Scanlan, M. J. Hynes, Equilibria in uranyl carbonate systems—I: The overall stability constant of $UO_2(CO_3)_3^{4-}$, *J. Inorg. Nucl. Chem*., 1977, **37**, 1013; b) J. P. Scanlan, Equilibria in uranyl carbonate systems—II: The overall stability constant of $UO_2(CO_3)_2^{2-}$ and the third formation constant of and the third formation constant of $UO_3(CO_3)_3^{4-}$, *J. Inorg. Nucl. Chem*., 1977, **39**, 635.

35 a) L. Ciavatta, D. Ferri, M. Grimaldi, R. Palombari, F. Salvatore, Dioxouranium (VI) carbonate complexes in acid solution, *J. Inorg. Nucl. Chem*., 1979, **41**, 1175; b) L. Ciavatta, D. Ferri, I. Grenthe, F. Salvatore, The first acidification step of the tris(carbonato)dioxouranate(VI) ion, $UO_2(CO_3)_3^{4-}$, *Inorg. Chem*., 1981, **20**, 463; c) L. Ciavatta, D. Ferri, I. Grenthe, F. Salvatore, K. Spahiu, Studies on Metal Carbonate Equilibria. 4. Reduction of the Tris(carbonato) dioxouranate(VI) Ion, $UO_2(CO_3)_3^{4-}$, in Hydrogen Carbonate Solutions, *Inorg. Chem*., 1983, **22**, 2088; d) I. Grenthe, K. Spahiu, G. Olofsson, Studies on metal carbonate equilibria. 9. Calorimetric determination of the enthalpy and entropy changes for the formation of uranium(IV and VI) carbonate complexes at 25 ℃ in a 3 M $(Na, H)ClO_4$ ionic medium, *Inorg. Chim. Acta*, 1984, **95**, 79; e) I. Grenthe, D. Ferri, F. Salvatore, G. Riccio, Studies on metal carbonate equilibria. Part 10. A solubility study of the complex formation in the uranium(VI)–water–carbon dioxide(g) system at 25 ℃, J. *Chem. Soc. Dalton Trans*., 1984, **1984**, 2439.

36 a) Z. Szabó, H. Moll, I. Grenthe, Structure and dynamics in the complex ion $(UO_2)_2(CO_3)(OH)_3^-$, *J. Chem. Soc. Dalton Trans*., 2000, **2000**, 3158; b) Z. Szabo, T. Toraishi, V. Vallet, I. Grenthe, Solution coordination chemistry of actinides: Thermodynamics, structure and reaction mechanisms, *Coord. Chem. Rev*., 2006, **250**, 784.

37 J. Y. Bourges, B. Guillaume, G. Koehly, D. E Hobart, J. R. Peterson, Coexistence of americium in four oxidation states in sodium carbonate-sodium bicarbonate medium, *Inorg. Chem*., 1983, **22**, 1179.

38 C. Nguyen-Trung, G. M. Begun, D. A. Palmer, Aqueous uranium complexes. 2. Raman spectroscopic study of the complex formation of the dioxouranium(VI) ion with a variety of inorganic and organic ligands, *Inorg. Chem*., 1992, **31**, 5280.

39 a) G. Meinrath, T. Kimura. Carbonate complexation of the uranyl(VI) ion, *J. Alloys Compd*., 1993, **202**, 89; b) G. Meinrath, T. Kimura, Behaviour of U(VI) solids under conditions of natural aquatic systems, *Inorg. Chim. Acta*, 1993, **204**, 79.

40 G. Bernhard, G. Geipel, T. Reich, V. Brendler, S. Amayri, H. Nitsche, Uranyl(VI) carbonate complex formation: Validation of the $Ca_2UO_2(CO_3)_3\ (aq.)$ species, Radiochim. Acta, 2001, 8, 511.

41 J. G. Catalano, G. E. Brown, Uranyl adsorption onto montmorillonite: Evaluation of binding sites and carbonate complexation, *Geochim. Cosmochim. Acta*, 2005, **69**, 2995.

42 W. M. Dong, S. C. Brooks, Determination of the Formation Constants of Ternary Complexes of Uranyl and Carbonate with Alkaline Earth Metals (Mg^{2+}, Ca^{2+}, Sr^{2+} and Ba^{2+}) Using Anion Exchange Method, *Environ. Sci. Technol*., 2006, **40**, 4689.

43 a) A. Ikeda, C. Hennig, S. Tsushima, K. Takao, Y. Ikeda, A. C. Scheinost, G. Bernhard, Comparative Study of Uranyl(VI) and (V) Carbonato Complexes in an Aqueous Solution, *Inorg. Chem*., 2007, **46**, 4212.; b) C. Hennig, A. Ikeda-Ohno, F. Emmerling, W. Kraus, G. Bernhard, Comparative investigation of the solution species $[U(CO_3)_5]^{6-}$, and the crystal structure of $Na_6[U(CO_3)_5] \cdot 12H_2O$, *Dalton Trans.*, 2010, **39**, 3744.

44 J. Cobos, T. Wiss, T. Gouder, V. V. Rondinella, XPS and SEM Studies on the Corrosion of UO_2 Cointaining Plutonium in Demineralized and Carbonated Water, *Mat. Res. Soc. Symp. Proc.*, 2002, **757**, 119.

45 T. Watanabe, Y. Ikeda, A Study on Identification of Uranyl Complexes in Aqueous Solutions Containing Carbonate Ion and Hydrogen Peroxide, *Energy Procedia*, 2013, **39**, 81.

46 D. M. Stanley, R. T. Wilkin, Solution equilibria of uranyl minerals: Role of the common groundwater ions calcium and carbonate, *J. Hazard. Mat*., 2019, **377**, 315.

47 R. S. Forsyth, L. O. Werme, Spent fuel corrosion and dissolution, *J. Nucl. Mater*., 1992, **90**, 3.

48 E. C. Pearcy, J. D. Prikryl, W. M. Murphy, B. W. Leslie, Alteration of Uraninite from the Nopal I Deposit, Peña Blanca District, Chihuahua, Mexico, Compared to Degradation of Spent Nuclear Fuel in the Proposed US High-Level Nuclear Waste Repository at Yucca Mountain, Nevada, *Appl. Geochem*., 1994, **9**, 713.

49 J. Bruno, I. Casas, E. Cera, R. C. Ewing, R. J. Finch, L. O. Werme, The Assessment of the Long-Term Evolution of the Spent Nuclear Fuel Matrix by Kinetic, Thermodynamic and Spectroscopic Studies of Uranium Minerals, *Mat. Res. Soc. Symp. Proc*., 1994, **353**, 633.

50 P. A. Finn, J. C. Hoh, S. F. Wolf, S. A. Slater, J. K. Bates, The Release of Uranium, Plutonium, Cesium, Strontium, Technetium and Iodine from Spent Fuel under Unsaturated Conditions, *Radiochim. Acta*, 1996, **74**, 65.

51 J. Bruno, R. C. Ewing, Spent Nuclear Fuel, *Elements*, 2006, **2**, 343.

52 R. C. Ewing, Long-term storage of spent nuclear fuel, *Nat. Mater*., 2015, **14**, 252.

53 B. E. Burakov, E. E. Strykanova, E. B. Anderson, Secondary uranium minerals on the surface of Chernobyl "lava", *Mat. Res. Soc. Symp. Proc*., 1999, **465**, 1309.

54 H. Amano, T. Matsunaga, S. Nagao, Y. Hanzawa, M. Watanabe, T. Ueno, Y. Onuma, The Transfer Capability of Long-Lived Chernobyl Radionuclides from Surface Soil to River Water in Dissolved Forms, *Org. Geochem*., 1999, **30**, 437.

55 E. C. Buck, J. C. Cunnane, N. R. Brown, N. L. Dietz, *Analytical Electron Microscopy Characterization of Uranium-Contaminated Soils from the Fernald Site,* FY1993 Report, Argonne National Laboratory, Argonne, Illinois, 1993.

56 D. E. Morris, P. G. Allen, J. M. Berg, C. J. Chisholm-Brause, S. Conradson, R. Donohoe, N. Hess, J. Musgrave, C. D. Tait, Speciation of Uranium in Fernald Soils by Molecular Spectroscopic Methods: Characterization of Untreated Soils, *Environ. Sci. Technol*., 1996, **30**, 2322.

57 S. F. Wolf, J. K. Bates, E. C. Buck, N. L. Dietz, J. A. Fortner, N. R. Brown, Physical and Chemical Characterization of Actinides in Soil from Johnston Atoll, *Environ. Sci. Technol.*, 1997, **31**, 467.

58 W. J. Deutsch, K. M. Krupka, M. J. Lindberg, K. J. Cantrell, C. F. Brown, H. T. Schaef, *Hanford Tanks 241-C-203 and 241-C-204: Residual Waste Contaminant Release Model and Supporting Data*, Report PNNL-14903, Pacific Northwest National Laboratory, Richland, Washington, 2004.

59 a) K. M. Krupka, H. T. Schaef, B. W. Arey, S, M. Heald, W. J. Deutsch, M. J. Lindberg, K. J. Cantrell, Residual Waste from Hanford Tanks 241-C-203 and 241-C-204. 1. Solids Characterization, *Environ. Sci. Technol*., 2006, **40**, 3749; b) K. J. Cantrell, K. M. Krupka, W. J. Deutsch, M. J. Lindberg, Residual Waste from Hanford tanks 241-C-203 and 241-C-

204. 2. Contaminant Release Model, *Environ. Sci. Technol*., 2006, **40**, 3755.
60 J. G. Catalano, J. Mckinley, J. M. Zachara, S. Heald, S. Smith, G. E. Brown, Changes in Uranium Speciation through a Depth Sequence of Contaminated Hanford Sediments, *Environ. Sci. Technol*., 2006, **40**, 2517.
61 P. C Burns, R. C Ewing, A. Navrotsky, Nuclear fuel in a reactor accident, *Science*, 2012, **335**, 1184.
62 R. M. Garrels, C. L. Christ, Behavior of Uranium Minerals During *Oxidation, US Geol. Surv. Prof. Pap*., 1959, **320**, 81.
63 a) C. Frondel, Mineral composition of gummite, *Am. Mineral*., 1956, **41**, 539; b) C. Frondel, Systematic mineralogy of uranium and thorium, *U.S. Geol. Surv. Bull*., 1958, **1064**, 1.
64 R. J. Finch, M. L. Miller, R. C. Ewing, Weathering of Natural Uranyl Oxide Hydrates: Schoepite Polytypes and Dehydration Effects, *Radiochim. Acta,* 1992, **58-59**, 433.
65 P. C. Burns, R. C. Ewing, M. L. Miller, Incorporation mechanisms of actinide elements into the structures of U^{6+} phases formed during the oxidation of spent nuclear fuel, *J. Nucl. Mater*., 1997, **245**, 1.
66 P. C. Burns, Cs boltwoodite obtained by ion exchange from single crystals: Implications for radionuclide release in a nuclear repository, *J. Nucl. Mater*., 1999, **265**, 218.
67 P. C. Burns, K. M. Deely, S. Skanthakumar, Neptunium incorporation into uranyl compounds that form as alteration products of spent nuclear fuel: Implications for geologic repository performance, *Radiochim. Acta*, 2004, **92**, 151.
68 A. L. Klingensmith, P. C. Burns, Neptunium substitution in synthetic uranophane and soddyite, *Am. Mineral*., 2007, **92**, 1946.
69 M. Douglas, S. B. Clark, S. Utsunomiya, R. C. Ewing, Cesium and strontium incorporation into uranophane, $Ca[(UO_2)(SiO_3OH)]_2 \cdot 5\,H_2O$, *J. Nucl. Sci. Technol*., 2002, **39**, 504.
70 W. M. Murphy, B. Grambow, Thermodynamic interpretation of neptunium coprecipitation in uranophane for application to the Yucca Mountain Repository, *Radiochim. Acta*, 2008, **96**, 563.
71 J. Plášil, A. R. Kampf, T. A. Olds, J. Sejkora, R. Škoda, P. C. Burns, J. Čejka, The new K, Pb-bearing uranyl-oxide mineral kroupaite: Crystal-chemical implications for the structures of uranyl-oxide hydroxy-hydrates, *Am. Mineral*., 2020, **105**, 561.
72 F. Cesbron, R. Pierrot, T. Verbeek, La roubaultite $Cu_2(UO_2)_3OH)_{10} \cdot 5\,H_2O$, une nouvelle espèce minérale, *Bull. Soc. Fr. Mineral. Cristallogr*., 1970, **93**, 550.
73 D. Ginderow, F. Cesbron, Structure de la roubaultite, $Cu_2(UO_2)_3(CO_3)_2O_2(OH)_2 \cdot 4\,H_2O$, *Acta Crystallogr. C*, 1985, **41**, 654.
74 M. Deliens, P. Piret, La fontanite, carbonate hydraté d'uranyle et de calcium, nouvelle espèce minérale de Rabejac, Hérault, France, *Eur. J. Mineral*., 1992, **4**, 1271.
75 K. Walenta, W. Wimmenauer, Der Mineralbestand des Michaelganges im Weiler bei Lahr (Schwarzwald), *Jh. Geol. Landesamt Baden-Württ*., 1961, **4**, 7.
76 K. Walenta, Widenmannit und Joliotit, zwei neue Uranyl-karbonatmineralien aus dem Schwarzwald, *Schweiz. Mineral. Petrogr. Mitt.*, 1976, **56**, 167.
77 K. Walenta, Grimselit ein neues Kalium-Natrium-Uranyl-Karbonat aus dem Grinselgebiet (Oberhasli, Kanton Bern, Schweiz), *Schweiz. Mineral. Petrogr. Mitt*., 1972, **52**, 93.
78 K. A. Hughes, P. C. Burns, A new uranyl carbonate sheet in the crystal structure of fontanite, $Ca[(UO_2)_3(CO_3)_2O_2] \cdot (H_2O)_6$, *Am. Mineral*., 2003, **88**, 962.
79 Y. Li, P. C. Burns, he crystal structure of synthetic grimselite, $K_3Na[(UO_2)(CO_3)_3] \cdot H_2O$. *Can. Mineral*., 2001, **39**, 1147.
80 Y. Li, S. V. Krivovichev, P. C. Burns, The crystal structure of $Na_4[(UO_2)(CO_3)_3]$ and its relationship to schröckingerite, *Mineral. Mag*., 2001, **65**, 297.
81 P. Škácha, J. Plášil, J. Sejkora, J. Čejka, R. Škoda, N. Meisser, Unique occurrence of bayleyite, $Mg_2[(UO_2)(CO_3)_3] \cdot 18\,H_2O$, from Jáchymov.*Bull. Mineral. Petrolog. Odd. Nár. Muz. (Praha*), 2014, **22**, 240.
82 J. Čejka, Z. Mrázek, Z. Urbanec, New data on sharpite, a calcium uranyl carbonate. *Neues Jb. Mineral. Monatshefte*, 1984, **1984**, 109.
83 J. Plášil, A unique structure of uranyl-carbonate mineral sharpite: A derivative of the rutherfordine topology, *Z. Kristallogr*., 2018, **233**, 579.
84 J. Plášil, J. Čejka, J. Sejkora, P. Škácha, V. Goliáš, P. Jarka, F. Laufek, J. Jehlička, I. Němec, L. Strnad, Widenmannite, a rare uranyl lead carbonate: occurrence, formation and characterization, *Mineral. Mag*., 2010, **74**, 97.
85 J. Plášil, L. Palatinus, J. Rohlíček, L. Houdková, M. Klementová, V. Goliáš, P. Škácha, Crystal structure of lead uranyl carbonate mineral widenmannite: Precession electron-diffraction and synchrotron powder-diffraction study, *Am. Mineral*., 2014, **99**, 276.
86 J. Plášil, K. Fejfarová, R. Skála, R. Škoda, N. Meisser, J. Hloušek, I. Císařová, M. Dušek, F. Veselovský, J. Čejka, J. Sejkora, P. Ondruš, The crystal chemistry of the uranyl carbonate mineral grimselite, $(K,Na)_3Na[(UO_2)(CO_3)_3] \cdot (H_2O)$, from Jáchymov, Czech Republic, *Mineral. Mag*., 2012, **76**, 443.
87 I. Císařová, R. Skála, P. Ondruš, M. Drábek, Trigonal $Na_4[(UO_2)(CO_3)_3]$, *Acta Crystallogr. E*, 2001, **57**, i32.
88 P. Ondruš, R. Skála, F. Veselovský, J. Sejkora, C. Vitti, Čejkaite, the triclinic polymorph of $Na_4[(UO_2)(CO_3)_3]$, - a new mineral, from Jachymov, Czech Republic, *Am. Mineral*., 2003, **88**, 686.
89 J. Čejka, J. Sejkora, J. Plášil, S. Bahfenne, S. J. Palmer, R. L. Frost, Raman spectroscopic study of the uranyl carbonate mineral čejkaite and its comparison with synthetic trigonal $Na_4[(UO_2)(CO_3)_3]$, *J. Raman Spectrosc*., 2010, **41**, 459.
90 J. Plášil, K. Fejfarová, M. Dušek, R. Škoda, J. Rohlíček, Revision of the symmetry and the crystal structure of čejkaite, $Na_4[(UO_2)(CO_3)_3$, *Am. Mineral*., 2013, **98**, 549.
91 A. R. Kampf, T. A. Olds, J. Plášil, P. C. Burns, J. Marty, Natromarkeyite and pseudomarkeyite, two new calcium-uranyl-carbonate minerals from the Markey mine, San Juan County, Utah, USA, Mineral. Mag., 2020, DOI: 10.1180/mgm.2020.59.
92 F. Mazzi, F. Rinaldi, Structural studies on $Me^{+}_{0-4}Me^{2+}_{2-0}UO_2(CO_3)_3 \cdot nH_2O$ compounds. I. The crystal structure of $K_3Na(UO_2)(CO_3)_3H_2O$, *Acta Crystallogr*., 1960, **13**, 1139.
93 N. J. Elton, J. J. Hooper, Widenmannite from Cornwall, England: the second world occurrence, *Mineral. Mag*., 1995, **59**, 745.
94 F. Colmenero, J. Cobos, V. Timón, Periodic DFT Study of the Structure, Raman Spectrum and Mechanical Properties of Schoepite Mineral, *Inorg. Chem*., 2018, **57**, 4470.
95 F. Colmenero, A. M. Fernández, J. Cobos, V. Timón, DFT Study of the Thermodynamic Properties and Stability of Schoepite and Metaschoepite Mineral Phases, *ACS Earth Space Chem*., 2019, **3**, 17.
96 F. Colmenero, A. M. Fernández, J. Cobos, V. Timón, Becquerelite Mineral Phase: Crystal Structure and Thermodynamic and Mechanic Stability by Using Periodic DFT, *RSC Adv*., 2019, **8**, 24599.
97 F. Colmenero, J. Plášil, J. Cobos, J. Sejkora, V. Timón, J. Čejka, L. J. Bonales, Crystal Structure, Hydrogen Bonding, Mechanical Properties and Raman Spectrum of the Lead

Uranyl Silicate Monohydrate Mineral Kasolite, *RSC Adv*., 2019, **9**, 15323.
98 F. Colmenero, J. Plášil, J. Sejkora, The Layered Uranyl Silicate Mineral Uranophane-β: Crystal Structure, Mechanical Properties, Raman Spectrum and Comparison with the α-Polymorph, *Dalton Trans*., 2019, **48**, 16722.
99 F. Colmenero, J. Plášil, J. Cobos, J. Sejkora, V. Timón, J. Čejka, A. M. Fernández, V. Petříček, Structural, Mechanical, Spectroscopic and Thermodynamic Characterization of the Copper-Uranyl Tetrahydroxide Mineral Vandenbrandeite, *RSC Adv*., 2019, **9**, 40708.
100 F. Colmenero, J. Plášil, I. Němec, Uranosphaerite: Crystal Structure, Hydrogen Bonding, Mechanics, Infrared and Raman Spectroscopy and Thermodynamics, *J. Phys. Chem. Solids*., 2020, **141**, 109400.
101 F. Colmenero, J. Plášil, P. Škácha, The magnesium uranyl tricarbonate octadecahydrate mineral, bayleyite: Periodic DFT study of its crystal structure, hydrogen bonding, mechanical properties and infrared spectrum, *Spectrochim. Acta A*, 2020, **234**, 118216.
102 F. Colmenero, J. Plášil, V. Timón, J. Čejka, Full crystal structure, hydrogen bonding and spectroscopic, mechanical and thermodynamic properties of mineral uranopilite, *RSC Adv*., 2020, 10, 31947.
103 F. Brivio, A. B. Walker, A. Walsh, Structural and electronic properties of hybrid perovskites for high-efficiency thin-film photovoltaics from first-principles, *APL Mater*., 2013, **1**, 042111.
104 R. Syariati, S. Minami, H. Sawahata, F. Ishii, First-principles study of anomalous Nernst effect in half-metallic iron dichloride monolayer, *APL Mater*, 2020, **8**, 041105.
105 E. J. Higgins , P. J. Hasnip, M. I. J. Probert, Simultaneous Prediction of the Magnetic and Crystal Structure of Materials Using a Genetic Algorithm, *Crystals*, 2019, 9, 439.
106 a) S. Ostanin, P. Zeller, Ab initio study of the uranyl oxide hydrates: a proton transfer mediated by water, *J. Phys.: Condens. Matter*., 2007, **19** 246108; b) S. Ostanin, P. Zeller, Ab initio study of uranyl peroxides: Electronic factors behind the phase stability, *Phys. Rev. B*, 2007, **75**, 073101.
107 P. F. Weck, E. Kim, Layered uranium(vi) hydroxides: structural and thermodynamic properties of dehydrated schoepite α-$UO_2(OH)_2$, *Dalton Trans*., 2014, **43**, 17191.
108 a) P. F. Weck, E. Kim, E. C. Buck, On the mechanical stability of uranyl peroxide hydrates: implications for nuclear fuel degradation, *RSC Adv*., 2015, **5**, 79090; b) P. F. Weck, E. Kim, Uncloaking the Thermodynamics of the Studtite to Metastudtite Shear-Induced Transformation, *J. Phys. Chem. C*, 2016, **120**, 16553.
109 D. A. Andersson, G. Baldinozzi, L. Desgranges, D. R. Conradson, S. R. Conradson, Density Functional Theory Calculations of UO_2 Oxidation: Evolution of UO_{2+X}, U_4O_{9-y}, U_3O_7, and U_3O_8, *Inorg. Chem*., 2013, **52**, 2769.
110 G. Beridze, P. M. Kowalski, Benchmarking the DFT+U Method for Thermochemical Calculations of Uranium Molecular Compounds and Solids, *J. Phys. Chem. A*, 2014, **118**, 11797.
111 T. M. Alam, Z. Liao, M. Nyman, J. Yates, Insight into Hydrogen Bonding of Uranyl Hydroxide Layers and Capsules by Use of 1H Magic-Angle Spinning NMR Spectroscopy, *J. Phys. Chem. C*, 2016, **120**, 10675.
112 a) N. Kalashnyk, D. L. Perry, F. Massuyeau, E. Faulques, Exploring Optical and Vibrational Properties of the Uranium Carbonate Andersonite with Spectroscopy and First-Principles Calculations, *J. Phys. Chem. C*, 2018, **12**, 7410; b) N. Kalashnyk, D. L. Perry, F. Massuyeau, E. Faulques, Spectroscopy and DFT studies of uranyl carbonate, rutherfordine, UO_2CO_3: a model for uranium transport, carbon dioxide sequestration, and seawater species, *J. Phys. D*, 2017, **50**, 505501; c) E. Faulques, D. L. Perry, N. Kalashnyk, Vibrational spectroscopy of a crystallographically unsettled uranyl carbonate: Structural impact and model, *Vib. Spectrosc*., 2018, **99**, 184; d) N. Kalashnyk, D. L. Perry, V. G. Ivanov, E. Faulques, Combined experimental and first-principles studies of a hydrated uranyl carbonate: Insight into phonon spectra for a core environmental class of uranium materials, *J. Phys. Chem. Solids*, 2020, **138**, 109260.
113 F. Colmenero, *Characterization of Secondary Phases of Spent Nuclear Fuel under Final Geological Disposal Conditions: Experimental and Theoretical Studies*, Ph. D. thesis, Universidad Autónoma de Madrid, Madrid, 2017, 443 pp.
114 L. J. Bonales, F. Colmenero, J. Cobos, V. Timón, Spectroscopic Raman Characterization of Rutherfordine: A Combined DFT and Experimental Study, *Phys. Chem. Chem. Phys*., 2016, **18**, 16575.
115 F. Colmenero, L. J. Bonales, J. Cobos, V. Timón, Study of the Thermal Stability of Studtite by In Situ Raman Spectroscopy and DFT Calculations, *Spectrochim. Acta A*, 2017, **174**, 245.
116 F. Colmenero, L. J. Bonales, J. Cobos, V. Timón, Structural, Mechanical and Vibrational Study of Uranyl Silicate Mineral Soddyite by DFT Calculations, *J. Solid State Chem*., 2017, **253**, 249.
117 F. Colmenero, L. J. Bonales, J. Cobos, V. Timón, Density Functional Theory Study of the Thermodynamic and Raman Vibrational Properties of γ-UO_3 Polymorph, *J. Phys. Chem. C*, 2017, **121**, 14507.
118 F. Colmenero, L. J. Bonales, J. Cobos, V. Timón, Thermodynamic and Mechanical Properties of the Rutherfordine, Mineral Based on Density Functional Theory, *J. Phys. Chem. C*, 2017, **121**, 5994.
119 F. Colmenero. A. M. Fernández, J. Cobos, V. Timón, Thermodynamic Properties of Uranyl Containing Materials Based on Density Functional Theory, *J. Phys. Chem. C*, 2018, **122**, 5254.
120 F. Colmenero, A. M. Fernández, J. Cobos, V. Timón, Temperature Dependent Free Energies of Reaction of Uranyl Containing Materials Based on Density Functional Theory, *J. Phys. Chem. C*, 2018, **122**, 5268.
121 F. Colmenero, L. J. Bonales, J. Cobos, V. Timón, Structural, mechanical and Raman spectroscopic characterization of layered uranyl silicate mineral uranophane-α by DFT methods, *Clay Miner*., 2018, **53**, 377.
122 F. Colmenero, Theoretical Studies of the Structural, Mechanic and Raman Spectroscopic Properties of Uranyl Containing Minerals, in *Minerals*, ed. K. S. Essa, InTechOpen, London, 2018, ch. 4; pp. 65−94.
123 F. Colmenero, The Application of Periodic Density Functional Theory to the Study of Uranyl Containing Materials: Thermodynamic Properties and Stability, in *Density Functional Theory*, ed. D. Glossman-Mitnik, InTechOpen, London, 2018, ch. 5; pp. 91−122.
124 F. Colmenero, Revealing Rutherfordine Mineral as an Auxetic Material, *Appl. Sci*., 2018, **8**, 2281.
125 F. Colmenero, J. Cobos, V. Timón, Negative Linear Compressibility in Uranyl Squarate Monohydrate, *J. Phys.: Condens. Matter*., 2019, **31**, 175701.
126 F. Colmenero, J. Cobos, V. Timón, Periodic density functional theory study of the Raman spectrum of the hydrated uranyl oxyhydroxide mineral becquerelite, *Theor. Chem. Acc*., 2019, **138**, 46.
127 S. J. Clark, M. D. Segall, C. J. Pickard, P. J. Hasnip, M. I. J. Probert, K. Refson, M. C. Payne, First Principles Methods Using CASTEP, *Z. Kristallogr*., 2005, **220**, 567.

128 X. Gonze, G.-M. Rignanese, M. Verstraetre, J.-M. Beuken, R. Pouillon, R. Caracas, A brief introduction to the ABINIT software package, *Z. Kristallogr*., 2005, **220**, 558.

129 P. Giannozzi, S. Baroni, N. Bonini, M. Calandra, R. Car, C. Cavazzoni, *et al*., QUANTUM ESPRESSO: a modular and open-source software project for quantum simulations of materials, *J. Phys.: Condens. Matter*, 2009, **21**, 395502.

130 F. Pascale, C. M. Zicovich-Wilson, F. López Gejo, B. Civalleri, R. Orlando, R. Dovesi, The calculation of the vibrational frequencies of crystalline compounds and its implementation in the CRYSTAL code, *J. Comput. Chem*., 2004, **25**, 888.

131 E. Artacho, E. Anglada, O. Diéguez, J. D. Gale, A. García, J. Junquera, R. M. Martin, P. Ordejón, J. M. Pruneda, D. Sánchez-Portal, J. M. Soler, The SIESTA method; developments and applicability, *J. Phys.: Condens. Matter*, 2008, **20**, 064208.

132 G. Kresse, J. Furthmüller, Efficient iterative schemes for ab initio total-energy calculations using a plane-wave basis set, *Phys. Rev. B*, 1996, **54**, 11169.

133 R. S. Lakes, Foam Structures with a Negative Poisson's Ratio, *Science*, 1987, **235**, 1038.

134 R. S. Lakes, Negative-Poisson's-Ratio Materials: Auxetic Solids, *Annu. Rev. Mater. Res*., 2017, **47**, 63.

135 R. H. Baughman, S. Stafström, C. Cui, S. O. Dantas, Materials with Negative Compressibilities in One or More Dimensions, *Science*, 1998, **279**, 1522.

136 A. B. Cairns, A. L. Goodwin, Negative Linear Compressibility, *Phys. Chem. Chem. Phys*., 2015, **17**, 20449.

137 K. E. Evans, A. Alderson, Auxetic Materials: Functional Materials and Structures from Lateral Thinking! *Adv. Mater*., 2000, **12**, 617.

138 G. M. Spinks, G. G. Wallace, L. S. Fifield, L. R. Dalton, A. Mazzoldi D. Rossi, L. Khayrullin, R. H. Baughman, Pneumatic Carbon Nanotube Actuators, *Adv. Mater*., 2002, **14**, 1728.

139 A.E. Aliev, J. Oh, M. E. Kozlov, A. A. Kuznetsov, S. Fang, A. F. Fonseca, R. Ovalle, M. D. Lima, M. H. Haque, Y. N. Gartstein, M. Zhang, A. A. Zakhidov, R. H. Baughman, Giant-Stroke, Superelastic Carbon Nanotube Aerogel Muscles, *Science*, 2009, **323**, 1575.

140 H. Abramovitch, M. Burgard, L. Edery-Azulay, K. E. Evans, M. Hoffmeister, W. Miller, F. Scarpa, C. W. Smith, K. F. Tee, Smart tetrachiral and hexachiral honeycomb: Sensing and impact detection, *Compos. Sci. Technol*., 2010, **70**, 1072.

141 b) J. N. Grima, R. Caruana-Gauchi, M. R. Dudek, K. W. Wojciechowski, R. Gatt, Smart metamaterials with tunable auxetic and other properties, *Smart Mater. Struct*., 2013, **22**, 084016; R. Gatt, L. Mizzi, J. I. Azzopardi, K. M. Azzopardi, D. Attard, A. Casha, J. Briffa, J. N. Grima, Hierarchical Auxetic Mechanical Metamaterials, *Sci. Rep*., 2015, **5**, 8395.

142 Materials Studio, http://3dsbiovia.com/products/collaborative-science/biovia-materials-studio/, accessed June 15, 2020.

143 M. C. Payne, M. P. Teter, D. C. Ailan, A. Arias, J. D. Joannopoulos, Iterative Minimization Techniques for Ab Initio Total-Energy Calculations: Molecular Dynamics and Conjugate Gradients, *Rev. Mod. Phys*., 1992, **64**, 1045.

144 N. Troullier, J. L. Martins, Efficient Pseudopotentials for Plane-Wave Calculations, *Phys. Rev. B*, 1991, **43**, 1993.

145 J. P. Perdew, K. Burke, M. Ernzerhof, Generalized Gradient Approximation Made Simple, *Phys. Rev. Lett*., 1996, **77**, 3865.

146 S. Grimme, Semiempirical GGA-type Density Functional Constructed with a Long-Range Dispersion Correction, *J. Comput. Chem*., 2006, **27**, 1787.

147 J. P. Perdew, A. Ruzsinszky, G. I. Csonka, O. A. Vydrov, G. E. Scuseria, L. A. Constantin, X. Zhou, K. Burke, Restoring the Density-Gradient Expansion for Exchange in Solids and Surfaces., *Phys. Rev. Lett.*, 2008, **100**, 136406.

148 F. Colmenero, V. Timón, Study of the structural, vibrational and thermodynamic properties of natroxalate mineral using density functional theory, *J. Solid State Chem*., 2018, **263**, 131.

149 P. F. Weck, M. E. Gordon, J. A. Greathouse, C. R. Bryan, S. P. Meserole, M. A. Rodriguez, M. C. Payne, E. Kim, Infrared and Raman spectroscopy of α-ZrW_2O_8: A comprehensive density functional perturbation theory and experimental study, J Raman Spectrosc., 2018, **49**, 1373.

150 M. Cococcioni, The LDA+U Approach: A Simple Hubbard Correction for Correlated Ground States, in *Correlated Electrons: From Models to Materials Modeling and Simulation*, Vol. 2, ed. Pavarini *et al*., Forschungszentrum Jülich, Berlin, 2012, ch. 4.

151 S. L. Dudarev, D. Nguyen-Manh, A. P. Sutton, Effect of Mott-Hubbard correlations on the electronic structure and structural stability of uranium dioxide, *Phil. Mag. B*, 1997, **75**, 613.

152 J. P. Crocombette, F. Jollet, L. T. Nga, T. Petit, Plane-wave pseudopotential study of point defects in uranium dioxide, *Phys. Rev. B*, 2001, **64**, 104107.

153 P. F. Weck, E. Kim, C. F. Jové-Colón, D. C. Sassani, On the role of strong electron correlations in the surface properties and chemistry of uranium dioxide, *Dalton Trans*., 2013, **42**, 4570.

154 B. G. Pfrommer, M. Cote, M. S. G. Louie, M. L. Cohen, Relaxation of Crystals with the Quasi-Newton Method, *J. Comp. Phys*., 1997, **131**, 233.

155 R. T. Downs, K. L. Bartelmehs, G. V. Gibbs, M. B. Boisen, Interactive Software for Calculating and Displaying X-Ray or Neutron Powder Diffractometer Patterns of Crystalline Materials, *Am. Mineral*., 1993, **78**, 1104.

156 J. F. Nye, *Physical Properties of Crystals*, Clarendon, Oxford, 1976.

157 R. Yu, J. Zhu, H. Ye, Calculations of Single-Crystal Elastic Constants Made Simple, *Comput. Phys. Commun*., 2010, **181**, 671.

158 a) F. Colmenero, Anomalous mechanical behavior of the deltic, squaric and croconic cyclic oxocarbon acids, *Mater. Res. Express*, 2019, **6**, 045610; b) F. Colmenero, Addendum: Anomalous mechanical behavior of the deltic, squaric and croconic cyclic oxocarbon acids, *Mater. Res. Express,* 2019, **6**, 069401.

159 a) F. Colmenero, Mechanical properties of anhydrous oxalic acid and oxalic acid dihydrate, *Phys. Chem. Chem. Phys*., 2019, **21**, 2673; b) F. Colmenero, Negative area compressibility in oxalic acid dihydrate, *Mater. Lett.,* 2019, **245**, 25.

160 a) F. Colmenero, Silver Oxalate: Mechanical Properties and Extreme Negative Mechanical Phenomena, *Adv. Theor. Simul*., 2019, **2**, 1900040; b) F. Colmenero, V. Timón, Extreme negative mechanical phenomena in the zinc and cadmium anhydrous metal oxalates and lead oxalate dihydrate, *J. Mater. Sci*., 2020, **55**, 218.

161 F. Colmenero, J. Sejkora, J. Plášil, Crystal Structure, Infrared Spectrum and Elastic Anomalies in Tuperssuatsiaite, *Sci. Rep*., 2020, **10**, 7510.

162 F. Colmenero, Organic acids under pressure: elastic properties, negative mechanical phenomena and pressure induced phase transitions in the lactic, maleic, succinic and citric acids, *Mater. Adv*., 2020, **1**, 1399.

163 A. Marmier, Z. A. D. Lethbridge, R. I. Walton, C. W. Smith, S. C. Parker, K. E. Evans, A Computer Program for the Analysis and Representation of Anisotropic Elastic Properties, *Comput. Phys. Commun*., 2010, **181**, 2102.

164 F. Birch, Finite Elastic Strain of Cubic Crystal. *Phys. Rev.*, 1947, **71**, 809.

165 R. J. Angel, Equations of State, *Rev. Mineral. Geochem*., 2000, **41**, 35.

166 EOSFIT 5.2 software, http://programming.ccp14.ac.uk/ccp/web-mirrors/ross-angel/crystal/software.html, accessed June 15, 2020.

167 M. J. Mélon, La Sharpite, nouveau carbonate d'uranyle du Congo belge, *Bulletin des Séances de l'Institut Royal Colonial Belge*, 1938, **9**, 333.

168 Ch. Halls, *Report on the mineralogy of a sample from the Agricola Resources Energy Ridge project, Hautuajaervi, Lapin Laani, Finland. Final Report*, Dept. of Mineralogy, NHM, London, 2005.

169 S. M. Carlson, G. W. Robinson, M. J. Elder, J. A. Jaszczak, T. J. Bornhorst, Greenockite and Associated Uranium-Vanadium, Minerals from the Huron River Uranium Prospect Baraga County, Michigan, *Rocks & Minerals*, 2007 **82**, 298.

170 K. Walenta, Grimselit von Menzenschwand, *Erzgräber*, 1995, **9**, 89.

171 a) P. Pauliš, S. Kopecký, P. Cérný, *Uranium Minerals of the Czech Republic and their Localities*, Martin Bartos, Kuttna, Czech Repubic, 2007, 132 pp.; b) J. Tvrdý, J. Plášil, Jáchymov - Reiche Erzlagerstätte und Radonbad im böhmischen Westerzgebirge, *Aufschluss*, 2010, **61**, 292.

172 K. A. H. Kubatko, P. C. Burns, The Rb analogue of grimselite, $Rb_6Na_2[(UO_2)(CO_3)_3] \cdot 2\,H_2O$, *Acta Crystallogr. C*, 2004, **60**, i25.

173 J. Sejkora, P. Pauliš, J, Jelínek, J. Vlk, The finds of čejkaite at mine adit of the uranium deposit Rožná, Czech Republic, *Bull. Mineral. Petrolog. Odd. Nár. Muz. (Praha)*, 2008, **16**, 212.

174 J. Abella, J. Viñals, Čejkaíta, arsenuranilita, compreignacita, natrozippeíta y otros minerales raros de uranio en la mina "Eureka" La Torre de Cabdella, Pallars Jussà, Lleida, *Rev. Mineral*., 2009, **2**, 52.

175 M. Castillo, L. Torró, M. Campeny, C. Villanova,E. Tauler, J. C. Melgarejo, Mineralogía del Depósito de Uranio Eureka (Castell-estaó, Pirineo, Cataluña), *Rev. Soc. Esp. Mineral*., 2009, **11**, 53.

176 J. G. Catalano, G. E. Brown, Analysis of uranyl-bearing phases by EXAFS spectroscopy: Interferences, multiple scattering, accuracy of structural parameters, and spectral difference, *Am. Mineral*., 2004, **89**, 1004.

177 F. Mouhat, F. X. Coudert, Necessary and Sufficient Elastic Stability Conditions in Various Crystal Systems, *Phys. Rev. B*, 2014, **90**, 224104.

178 M. Born, On the Stability of Crystal Lattices, *Math. Proc. Cambridge Phil. Soc*., 1940, **36**, 160.

179 W. Voigt, *Lehrbuch der Kristallphysik*, Teubner, Leipzig, 1962.

180 A. Reuss, Berechnung der Fliessgrenze von Mischkristallen auf Grund der Plastizitatsbedingung fur Einkristalle, *Z. Angew. Math. Mech*., 1929, **9**, 49.

181 R. Hill, The Elastic Behaviour of a Crystalline Aggregate, *Proc. Phys. Soc. Lond. A*, 1952, **65**, 349.

182 S. F. Pugh, XCII. Relations between the Elastic Moduli and the Plastic Properties of Polycrystalline Pure Metals, *Phil. Mag*., 1954, **45**, 823.

183 Y. Bouhadda, S. Djella, M. Bououdina, Y. Fenineche, Y. Boudouma, Structural and Elastic Properties of LiBH_4 for Hydrogen Storage Applications, *J. Alloys Compd*., 2012, **534**, 20.

184 H. Niu, P. Wei, Y. Sun, C. X. Chen, C. Franchini, D. Li, Y. Li, Electronic, Optical, and Mechanical Properties of Superhard Cold-Compressed Phases of Carbon, *Appl. Phys. Lett*., 2011, **99**, 031901.

185 S. I. Ranganathan, M. Ostoja-Starzewski, Universal Elastic Anisotropy Index, *Phys. Rev. Lett*., 2008, **101**, 055504.

186 Z. A. D. Lethbridge, R. I. Walton, A. S. H. Marmier, C. W. Smith, K. E. Evans, Anisotropy and Extreme Poisson's Ratios in Single Crystals, *Acta Mater.*, 2010, **58**, 6444.